Kilowatt-scale CO electroreduction enabled by cation-induced double-layer rigidity control

Wenzhi Teng[1,3], Mengjiao Zhuansun[1,3], Haoxiang Bai[1,3], Xuewei Hao[1], Yu Yang[2], Zhuo Chen[1], Fengwang Li[2], Lu Wang[1], Yuhang Wang[1*]

[1] *Institute of Functional Nano & Soft Materials (FUNSOM), Soochow University, 199 Ren'ai Road, Suzhou, Jiangsu, 215123, China.*

[2]*School of Chemical and Biomolecular Engineering and ARC Centre of Excellence for Green Electrochemical Transformation of Carbon Dioxide, The University of Sydney, Sydney, NSW 2006, Australia.*

[3]*These authors contributed equally to this work.*

[*]Correspondence should be addressed to Yuhang Wang (*yhwang1988@suda.edu.cn*).

Experimental

Electrode preparation

The reinforced gas diffusion electrode (GDE) was prepared by spraying a CB ink mixed with a polytetrafluoroethylene (PTFE) dispersion (60 wt.% dispersion, Aladdin) onto commercial carbon paper. Specifically, the PTFE-CB ink was prepared by mixing 0.1 g of CB (Vulcan XC-72R, SCI Materials Hub) with PTFE (25% of the CB mass) in 50 mL of methanol. After ultrasonication for 2 hours, the ink was air-sprayed onto the gas diffusion layer (GDL) (Sigracet 28 BC, SCI Materials Hub) at 60°C. The reinforced GDL was then sintered in a muffle furnace at 300°C for 10 minutes. A layer of PTFE was sprayed onto the back of the treated electrode to enhance hydrophobicity.

The cathode was fabricated by sequentially spraying the catalyst ink onto the reinforced GDL, followed by an additional layer of CB ink. The catalyst ink was prepared by dispersing 400 mg of Cu nanoparticles (Sigma-Aldrich) and 100 μL of Nafion ionomer (Sigma Aldrich, 5wt.% in

lower aliphatic alcohols and water) in 25 mL of methanol. CB ink was prepared by dispersing 100 mg of CB and 100 μL of Nafion ionomer in 25 mL of methanol. Both the Cu and CB inks were ultrasonicated for 2 hours before being sequentially air-sprayed onto the reinforced GDL at 60°C to fabricate the cathode.

The anode was prepared by electrodepositing NiFe hydroxides. Nickel foam (0.3 mm, Suzhou Suke Lean Instrument Co., Ltd) was immersed in a solution containing 3 mM $Ni(NO_3)_2 \cdot 6H_2O$ (Sigma Aldrich) and 3 mM $Fe(NO_3)_3 \cdot 9H_2O$ (Sigma Aldrich). During the electrodeposition process, a platinum wire was used as the counter electrode, and an Ag/AgCl was employed as the reference electrode. The electrochemical workstation (DH7002A, Donghua Analytical Instruments (Taizhou) Co., Ltd.) was used to apply a potential of −1.0 V vs. Ag/AgCl for 5 minutes. After deposition, the NiFe electrode was rinsed with acetone and deionized water.

Material characterizations

Scanning electron microscopy (SEM) imaging and Energy dispersive X-ray (EDX) elemental mapping were performed via a high-resolution scanning electron microscope (G500; Zeiss).

Structural characterizations were performed using X-ray diffraction (XRD, PANalytical X'Pert Pro).

Static contact angle measurements were performed via the sessile drop method on a video-based measurement system. The measurements were performed by (1) placing a droplet of water onto a square-shaped specimen extracted from a GDE of interest, (2) fitting a tangent line to the intersection of the solid, liquid, and gas phases using software, and (3) determining the external angle using software.

K^+ retention measurements were carried out in 1 M KOH using a two-electrode configuration in a beaker. The measurements were performed by following a procedure similar to that described in ref. 1. A Pt electrode was used as the counter electrode and a GDE with a catalyst of interest (with a geometric area of 1 cm × 1.5 cm) was used as the working electrode. The back side of the GDE was fully covered with a Kapton type. Constant full cell potentials of −2.2 V were applied immediately before immersing the GDE into 1 M KOH. The GDE was taken out of the solution after 120 s and transferred to a vial with 10 ml deionized water before releasing the applied potential. Then, any absorbed K^+ on the GDE was released into the deionized water. The amount of K^+ in the water was detected using an inductively coupled plasma optical emission spectrometer detector (Avio 200; PerkinElmer) that enabled coverage of the full wavelength (167 and 785 nm). The K^+ concentration was normalized by ECSA.

In-situ Raman experiment

In-situ Raman spectroscopy measurements on all Cu or Cu-X electrodes were carried out using the Renishaw inVia Qontor Raman microscope in an open flow cell. Raman spectra were recorded using a Renishaw Raman spectrometer and analyzed and averaged using WiRE 4.4 software. Each Raman spectrum presented in this work is an average of more than 4 scans with an acquisition time of 20 s. The setup contains a 633 nm excitation laser and a 1200 mm^{-1} grating. The laser power was 200 μW with an intensity of 1%, and a telephoto objective with 50× magnification was used. A Pt wire was used as the counter electrode, and an Ag/AgCl electrode served as the reference electrode. The CO flow rate was about 1 sccm cm^{-2}. 18-Crown-6 chelated 0.1 M KOH, 0.1 M KOH, 0.1 M KOH + 0.1 M K_2SO_4, 0.1 M KOH + 0.2 M K_2SO_4, 0.1 M KOH + 0.2 M K_2SO_4, 0.1 M KOH + 0.45 M K_2SO_4 or 1 M KOH was used as the electrolyte.

Electrochemical measurements

For watt-scale electrolysis, electrochemical experiments were performed in a zero-gap MEA

electrolyzer (5 cm^2, Dioxide Materials Corporation). Humidified CO is continuously fed into the cathode gas chamber at a rate of 40 sccm controlled by a digital mass flow controller (CS200A, from Sevenstar Flow (Beijing) Co., Ltd). Pure water (Milli-Q pure water meter) or KOH (≥99%, Aldrich) solution was passed through a peristaltic pump into the anode liquid chamber at a rate of 10 ml min^{-1}. The anode adopts a self-made NiFe electrode. An anion exchange membrane (AEM) (Fumasep FAA-3-50) was placed between the cathode and anode. Electrochemical measurements were conducted using a DH7002 potentiostat (from Donghua Analytical Instruments (Taizhou) Co., Ltd.). Chronopotentiometry (V~t) measurements were carried out at current densities ranging from 20 to 780 mA cm^{-2}.

For kilowatt-scale electrolysis, the same Fumasep FAA-3-50 and NiFe anode as the 5 cm^2 electrolysis test was used. The electrolyte was 1 M KOH. The cathode was supplied with humidified CO at 4 ml cm^{-2} min^{-1}, and the anolyte circulating rate was 100 mL min^{-1}. The circulating cooling water was used for experiments with heat management. The measurements were performed using a HE80 potentiostat (Ivium Technologies B.V.) or a DC power supply (csyj48-150, COSYEN) with chronoamperometry (V~t) measurements conducted in the 100-500 mA cm^{-2} range. The gas products were analyzed by inline gas chromatography (GC2060, Wuhao Information Technology (Shanghai) Co., Ltd.). A thermal conductivity detector (TCD) analyzed the gaseous products (CO and H_2) generated at the cathode outlet. A flame ionization detector (FID) detected the gaseous products(C_2H_4) generated at the cathode outlet. Analysis of liquid products was performed using high-performance liquid chromatography (HPLC, Vanquish Core, ThermoFisher). The gas and liquid products were calibrated by an external standard method. The values reported are averages of at least three replicates with standard deviations as the error bars.

CORR product analyses

The FE for gaseous products was calculated by using the following equation:

$$\mathrm{FE}(\%) = \frac{F \times n \times V_{\mathrm{gas}} \times c}{i \times V_{\mathrm{m}}} \quad (1)$$

Where F represents the Faraday constant, n represents the number of electrons transferred, V_{gas} represents the gas flow rate, c represents the detected concentration of gaseous production, i represents the total current, and V_{m} represents the unit molar volume of the product of interest. The flow rate at the cathode outlet was measured using a bubble flow meter.

The FE for liquid products was calculated as follows:

$$\mathrm{FE}(\%) = \frac{N \times F \times n_{\mathrm{product}}}{Q} \quad (2)$$

Where nproduct represents the total number of moles of product and Q = i×t represents the total charge passing during measurement.

EE was calculated as follows:

$$\mathrm{EE} = \frac{E_{\mathrm{cell}}^{0}}{\mathrm{E}_{\mathrm{cell}}} \times \mathrm{FE}_{\mathrm{product}} \times 100\% \quad (3)$$

where E_{cell}^{0} represents the thermodynamic cell potential for products (ethylene E_{cell}^{0} = 1.06 V; ethanol E_{cell}^{0} = 1.04 V; propanol E_{cell}^{0} = 1.03 V; acetate E_{cell}^{0} = 0.78 V).

COMSOL modeling

The local concentrations of K^+ and CO at the catalyst layer with the CB layer were modeled in COMSOL (COMSOL Multiphysics version 5.5) using a 1D reaction-diffusion model. The Secondary Current Distribution and Transport of Diluted Species physics modules within COMSOL were used to model the interactions between K^+ and CO in a time-dependent study.

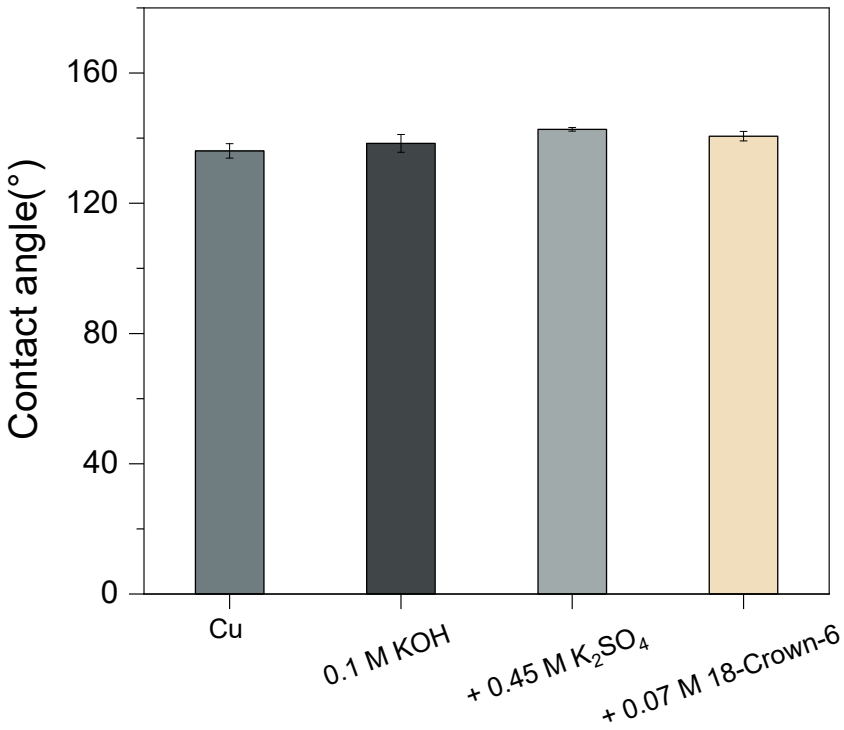

Fig. S1 Contact angles measured on the Cu catalyst surface before and after CORR testing in different electrolytes: pristine 0.1 M KOH, 0.1 M KOH + 0.45 M K_2SO_4, and 0.1 M KOH + 0.07 M 18-Crown-6.

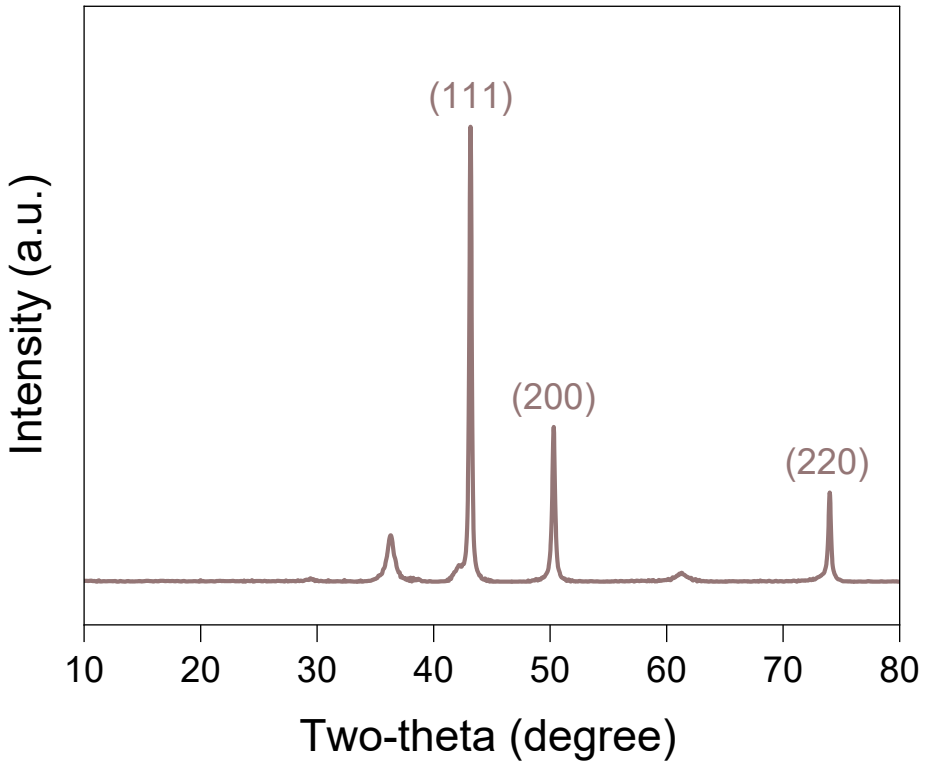

Fig. S2 X-ray diffraction (XRD) pattern of the as-received Cu nanoparticles, showing peaks corresponding to the (111), (200), and (220) planes of metallic copper.

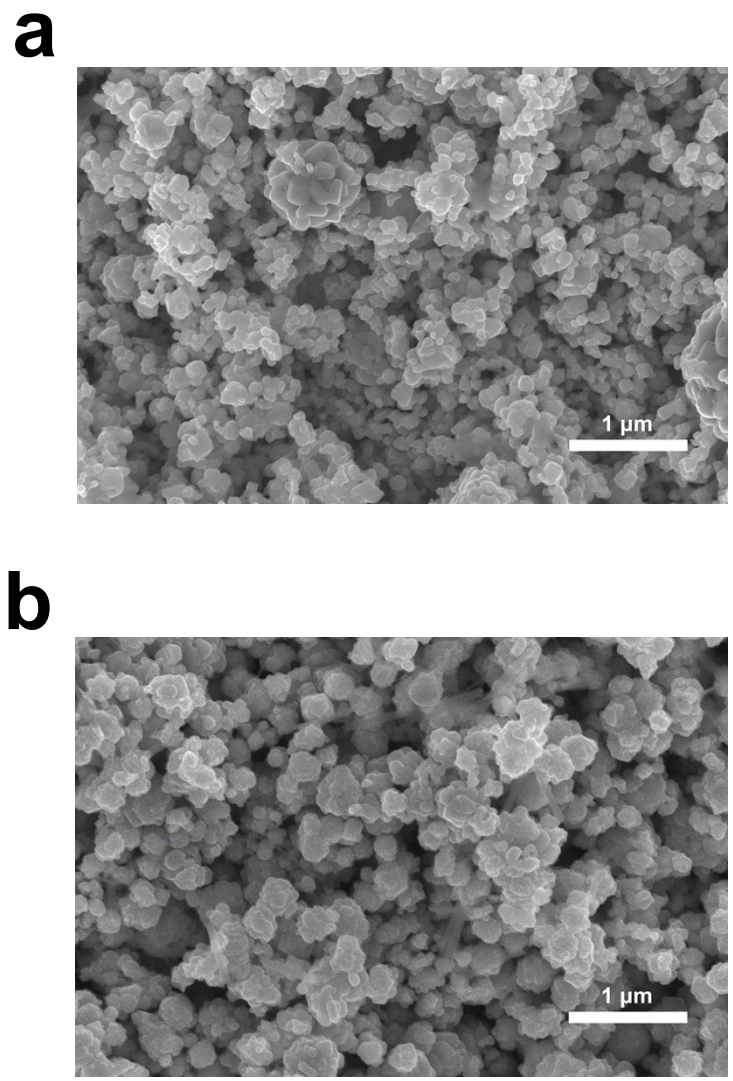

Fig. S3 Representative scanning electron microscopy (SEM) images of the Cu catalyst (a) before and (b) after CORR testing.

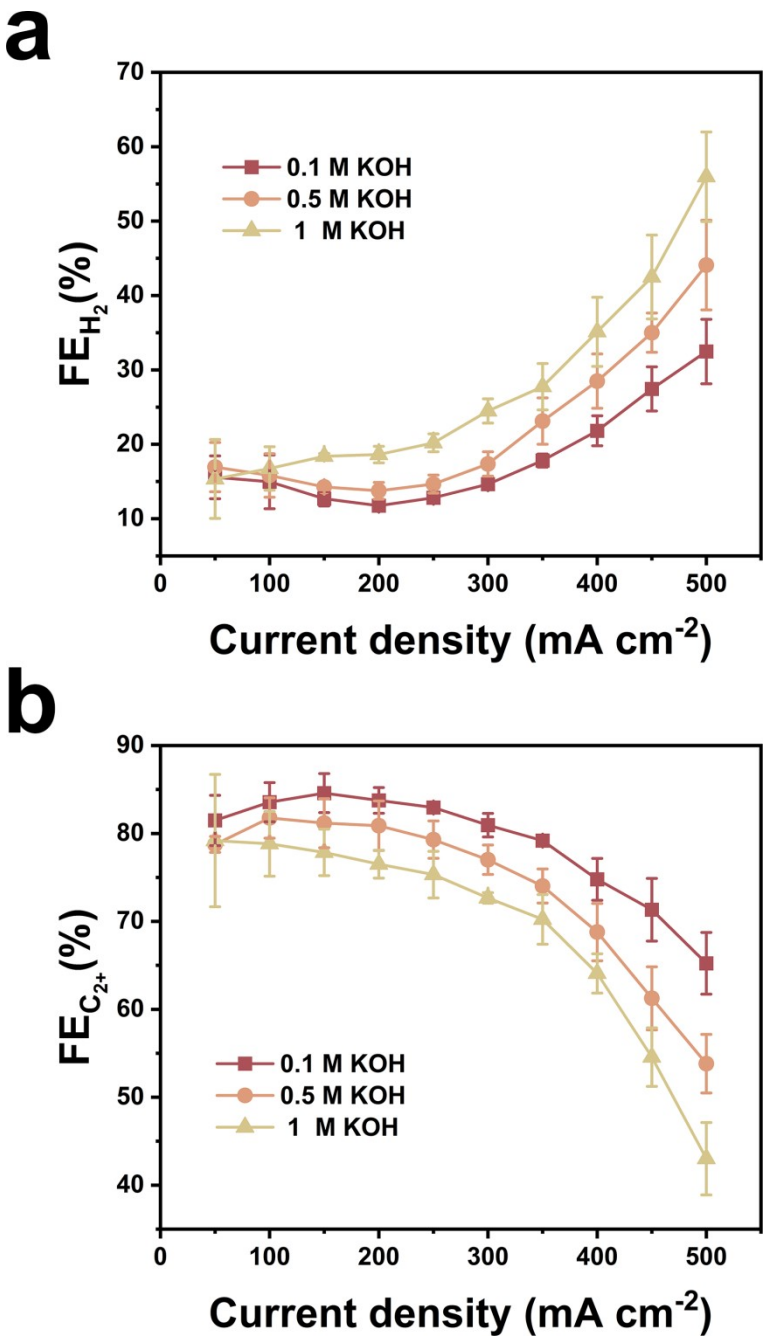

Fig. S4 FEs of (a) H_2 and (b) C_{2+} products in MEA electrolyzers using different concentrations of KOH anolytes. Error bars represent the standard deviations of at least three independent measurements.

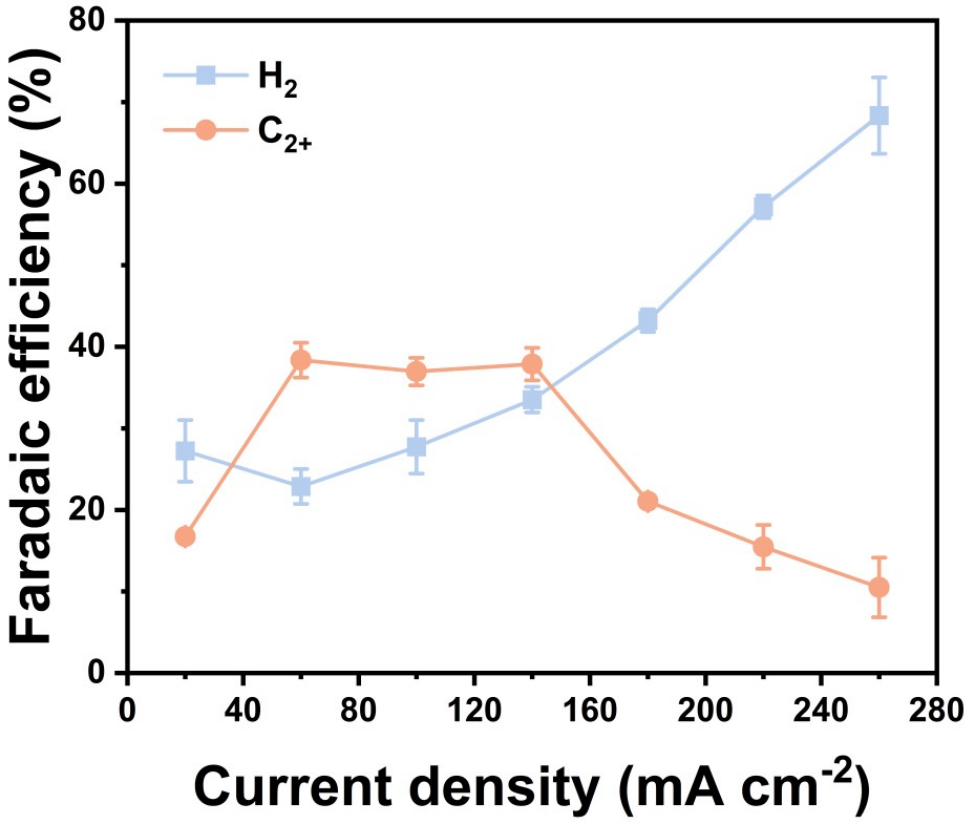

Fig. S5 FEs of H_2 and C_{2+} products in CO electrolyzers using pure water anolytes. Error bars represent the standard deviations of at least three independent measurements.

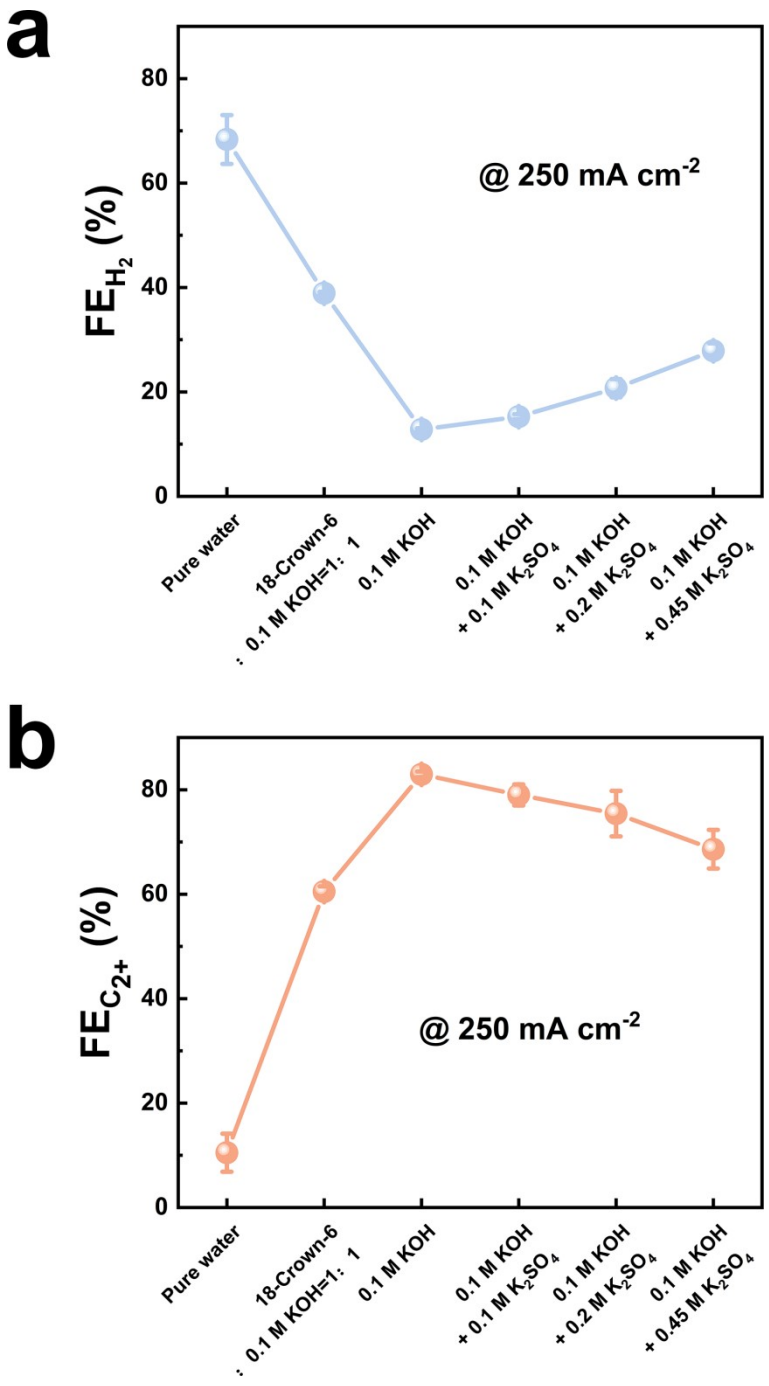

Fig. S6 FEs of (a) H_2 and (b) C_{2+} products as functions of K^+ concentrations at 250 mA cm^{-2}. Error bars represent the standard deviations of at least three independent measurements.

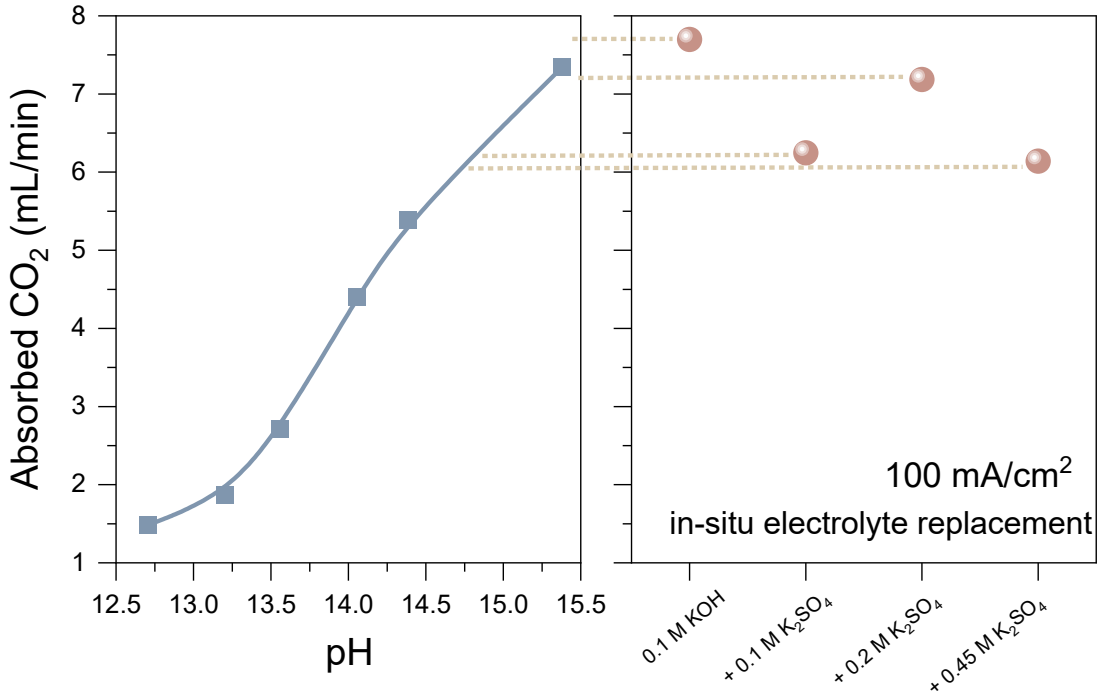

Fig. S7 Local pH during CO reduction and its invariance with bulk K^+ concentration. Calibration curve (left): CO_2 capture rate (measured as ml min^{-1}) as a function of bulk electrolyte pH under open-circuit conditions (no applied current). Determination of local pH during operation (right): The measured CO_2 capture rates during CO_2 reduction at 100 mA cm^{-2}, following in-situ exchange to electrolytes with varying total K^+ concentrations (1 M, 0.5 M, 0.3 M, 0.1 M). Horizontal dashed lines connect these operational data points to the calibration curve, indicating the corresponding local pH values

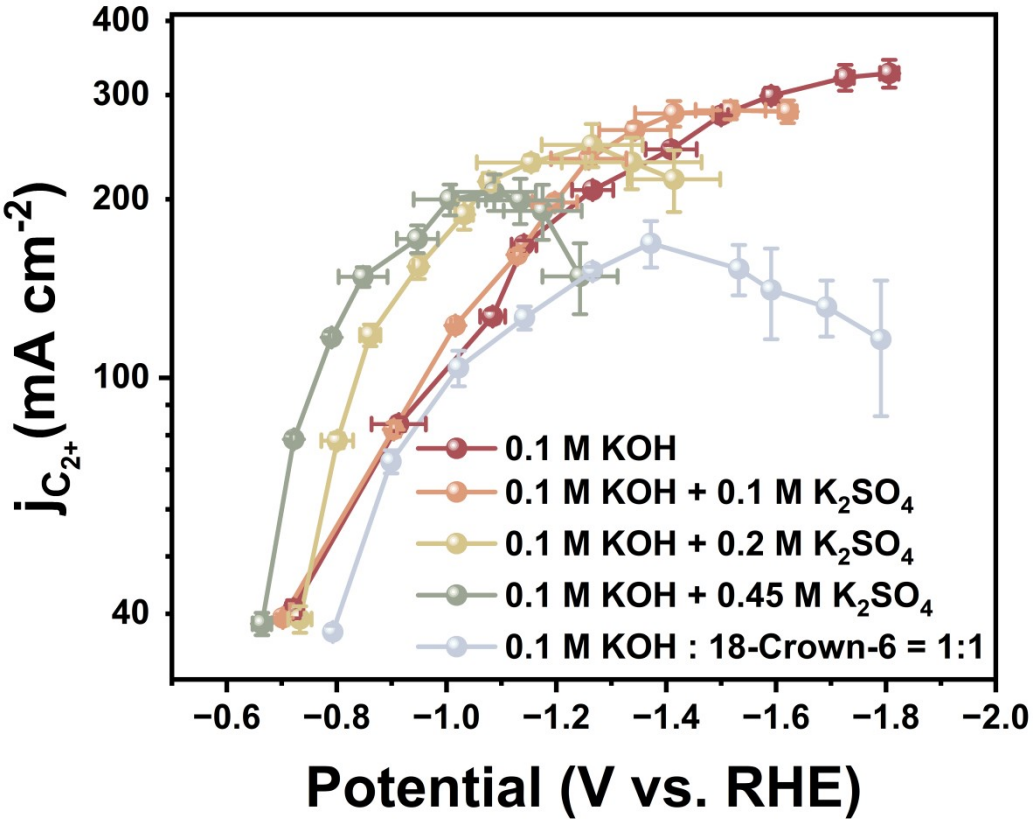

Fig. S8 Comparison of the partial current density of C_{2+} products.

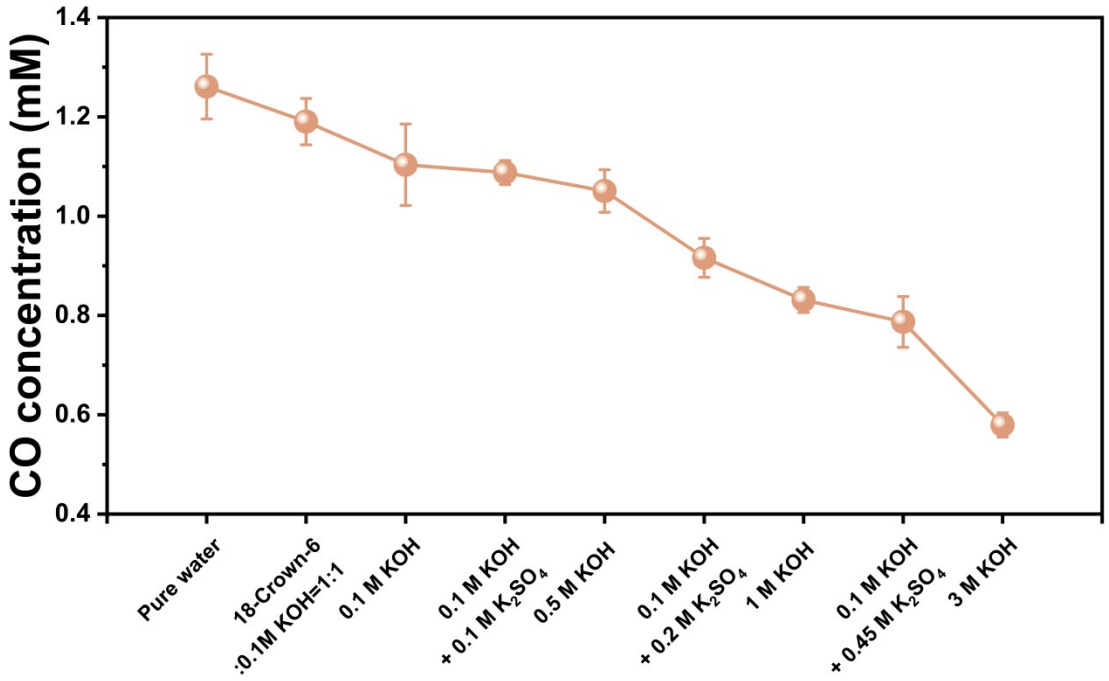

Fig. S9 The solubility of CO in different solutions. Error bars represent the standard deviations of at least three independent measurements.

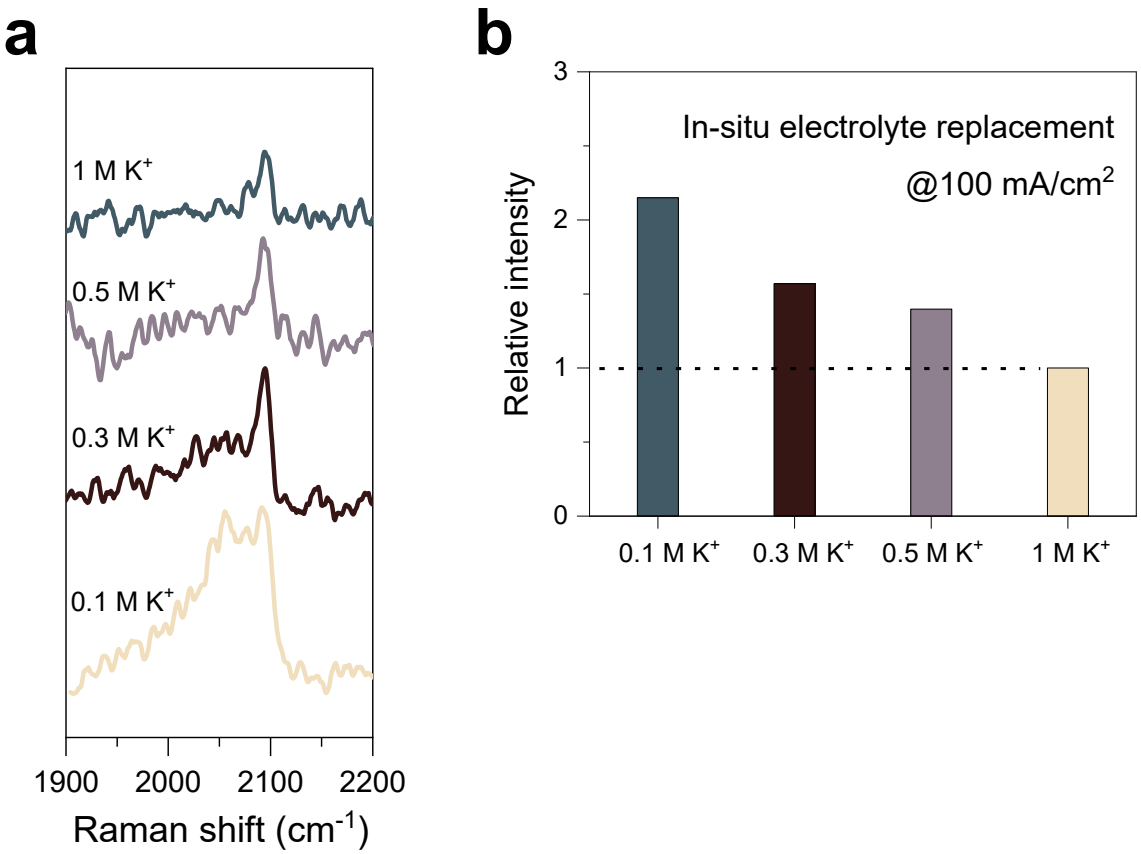

Fig. S10 *CO surface coverage at reduced K^+ concentrations. (a) In situ Raman spectra showing the adsorbed CO (*CO) band in the ~2050-2100 cm^{-1} region, measured during CO electrolysis at 100 mA cm^{-2} in a custom MEA electrolyzer. Spectra were acquired in electrolytes with a fixed 0.1 M KOH concentration and varying amounts of K_2SO_4 to achieve total K^+ concentrations of 1 M, 0.65 M, 0.45 M, and 0.1 M. (b) Integrated intensity of the *CO band from (a), normalized to the value at 1 M K^+.

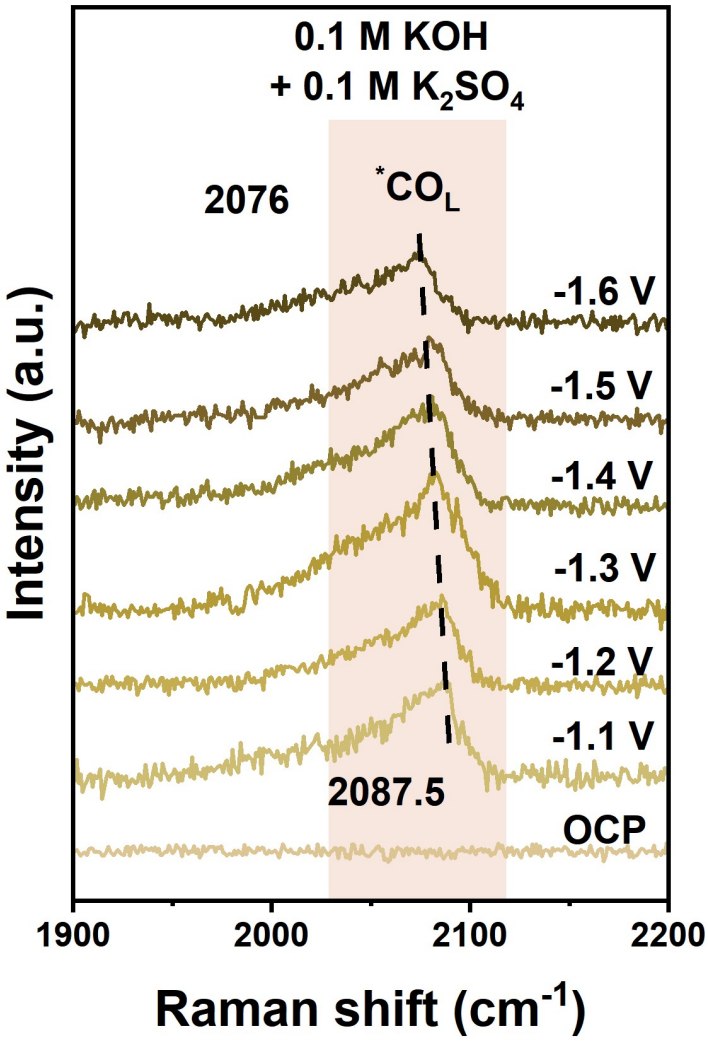

Fig. S11 In-situ Raman spectra collected using Cu-PTFE electrodes in 0.1 M KOH + 0.1 M K_2SO_4 anolytes.

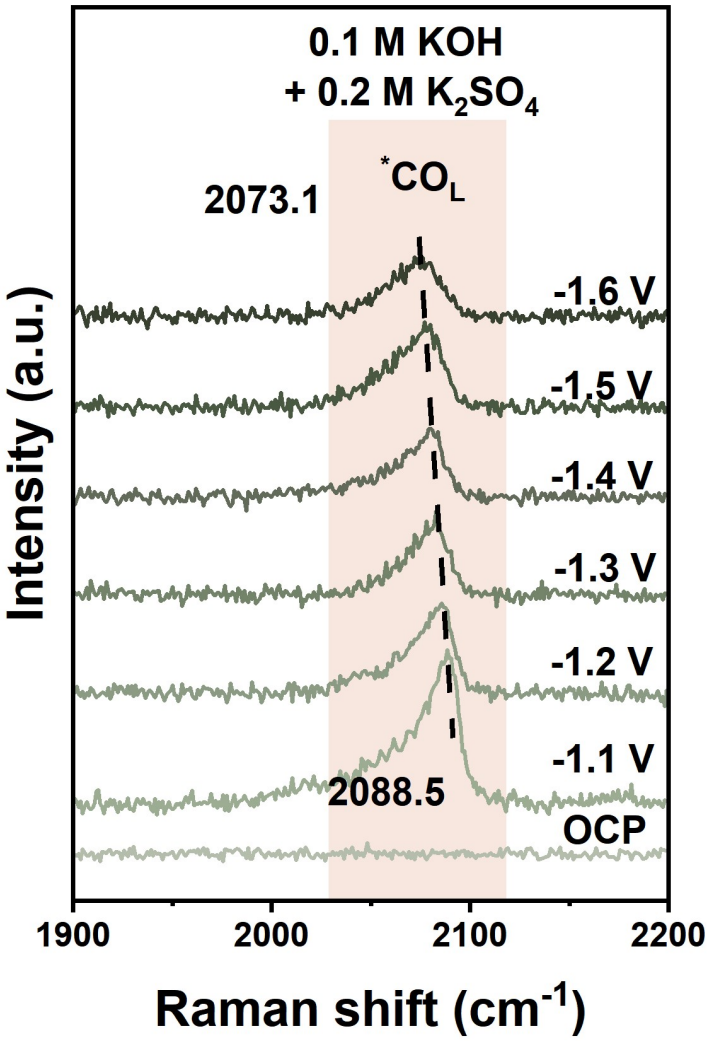

Fig. S12 In-situ Raman spectra collected using Cu-PTFE electrodes in 0.1 M KOH + 0.2 M K_2SO_4 anolytes.

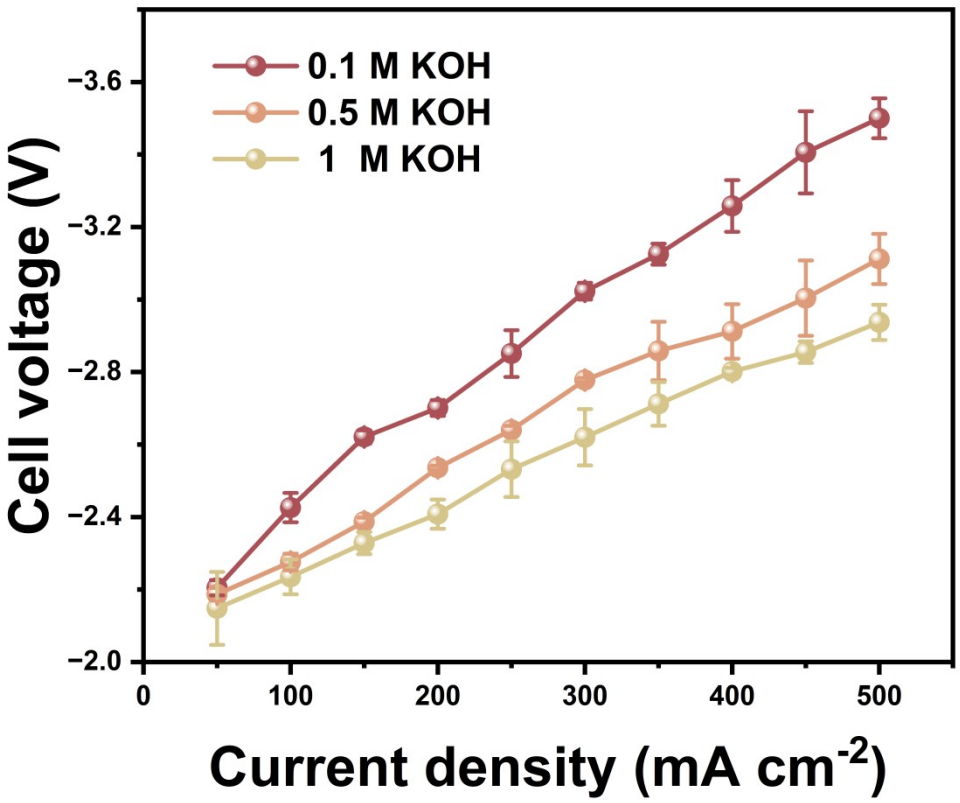

Fig. S13 Cell voltage during testing in MEA with different concentrations of KOH anolytes. Error bars represent the standard deviations of at least three independent measurements.

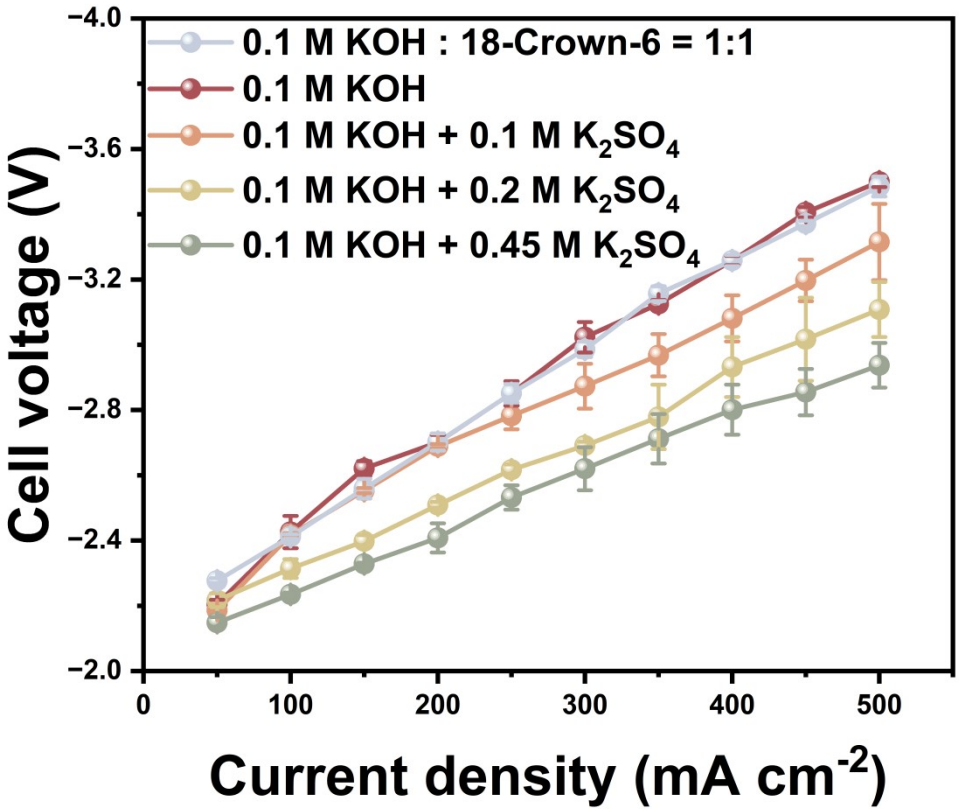

Fig. S14 Cell voltage during testing in MEA with different concentrations of K^+ anolytes. Error bars represent the standard deviations of at least three independent measurements.

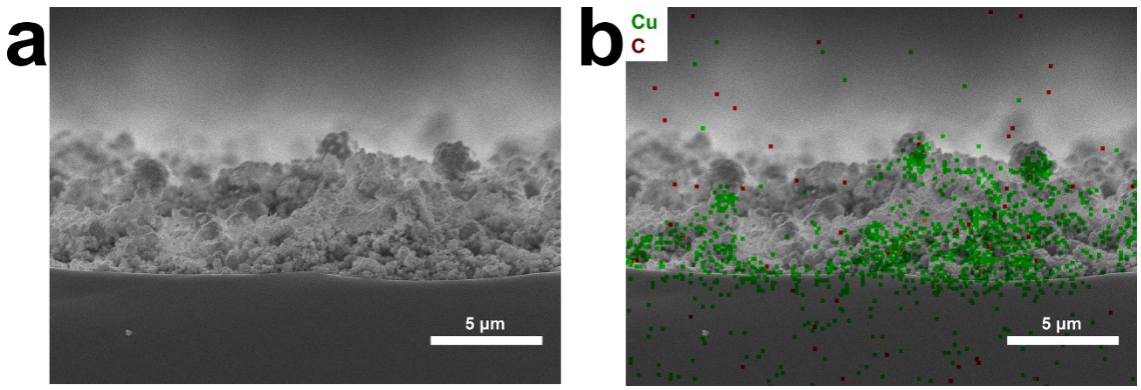

Fig. S15 Cu CL thickness determination. (a) The cross-section SEM image of a Cu electrode (b) The cross-section C and Cu elemental mapping images of the Cu electrode.

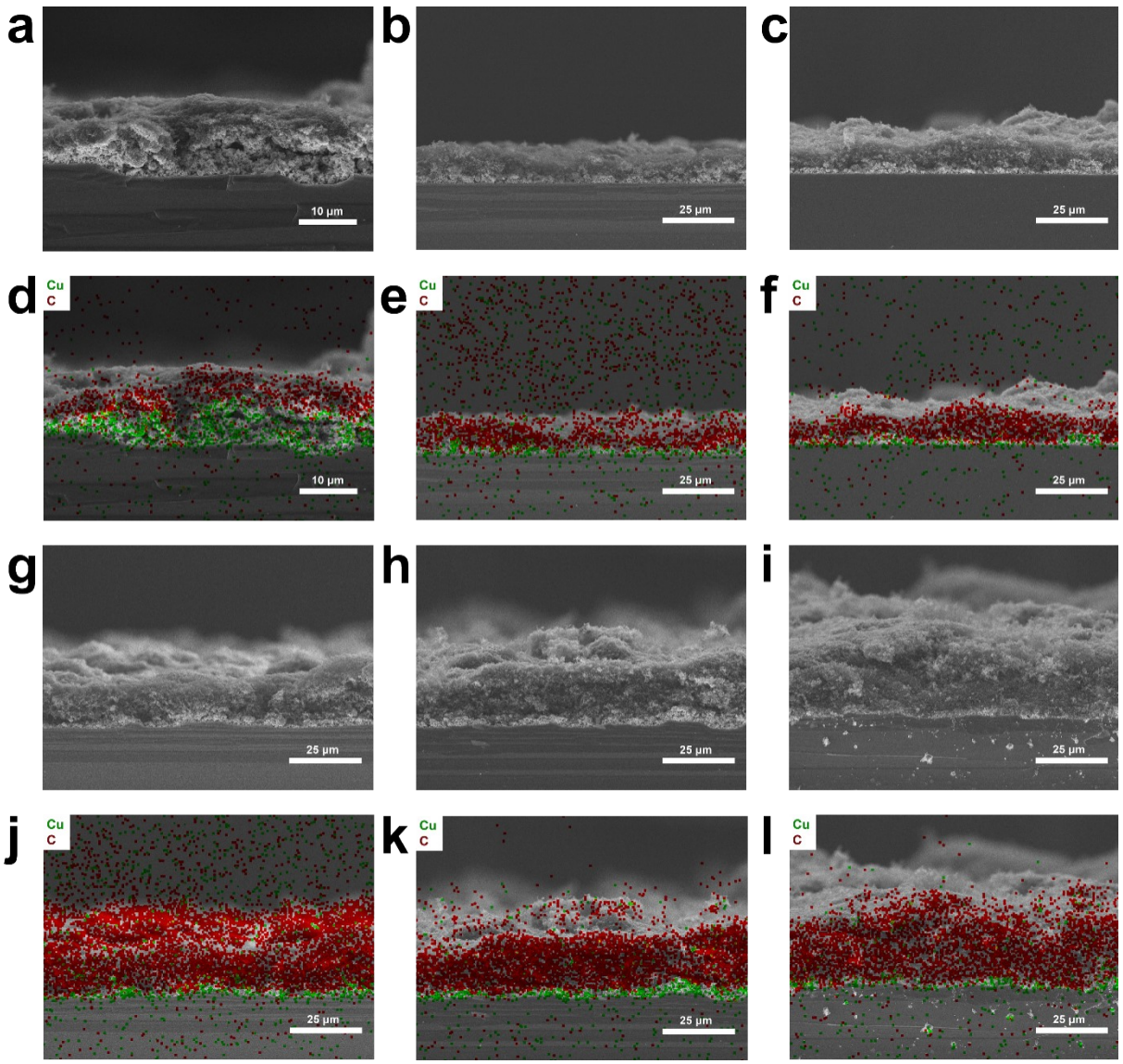

Fig. S16 Determination of the CB layer thickness. Cross-section SEM images of (a) Cu-3, (b) Cu-6, and (c) Cu-9 electrode. Cross-section C and Cu elemental mapping images of (d) Cu-3, (e) Cu-6, and (f) Cu-9 electrode. Cross-section SEM images of (g) Cu-12, (h) Cu-18, and (i) Cu-24 electrode. Cross-section C and Cu elemental mapping images of (j) Cu-12, (k) Cu-18, and (l) Cu-24 electrode.

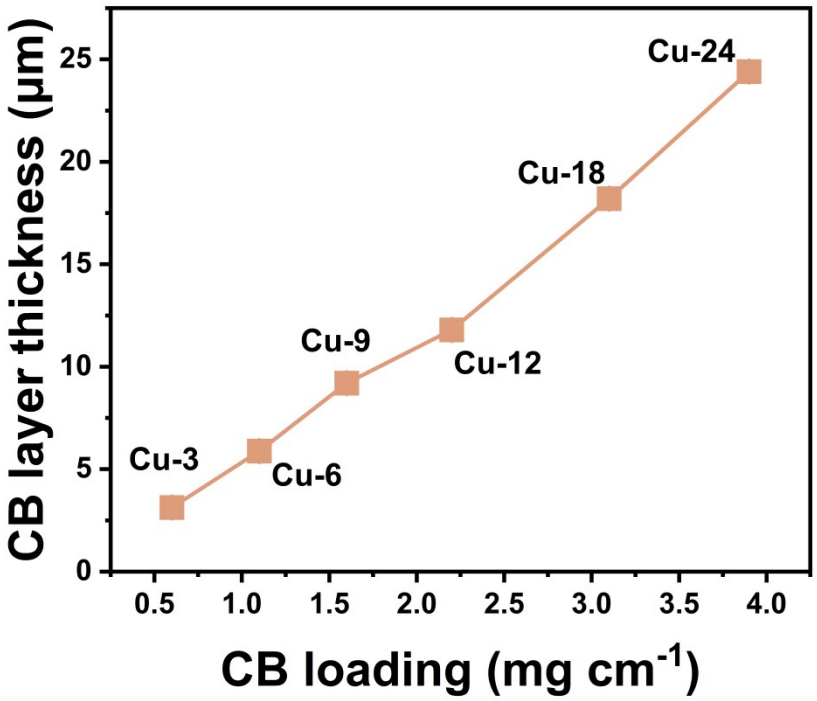

Fig. S17 The correlation between CB layer thicknesses and their mass loadings. Error bars represent the standard deviations of at least three independent measurements.

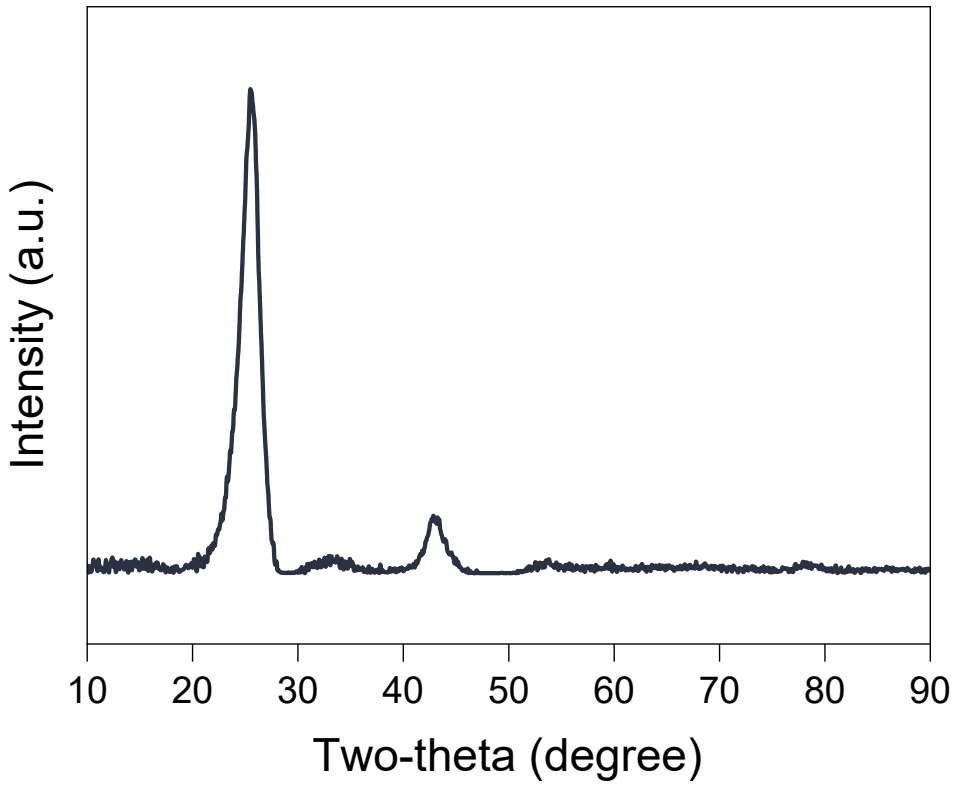

Fig. S18 XRD pattern of carbon black (Vulcan-XC-72R).

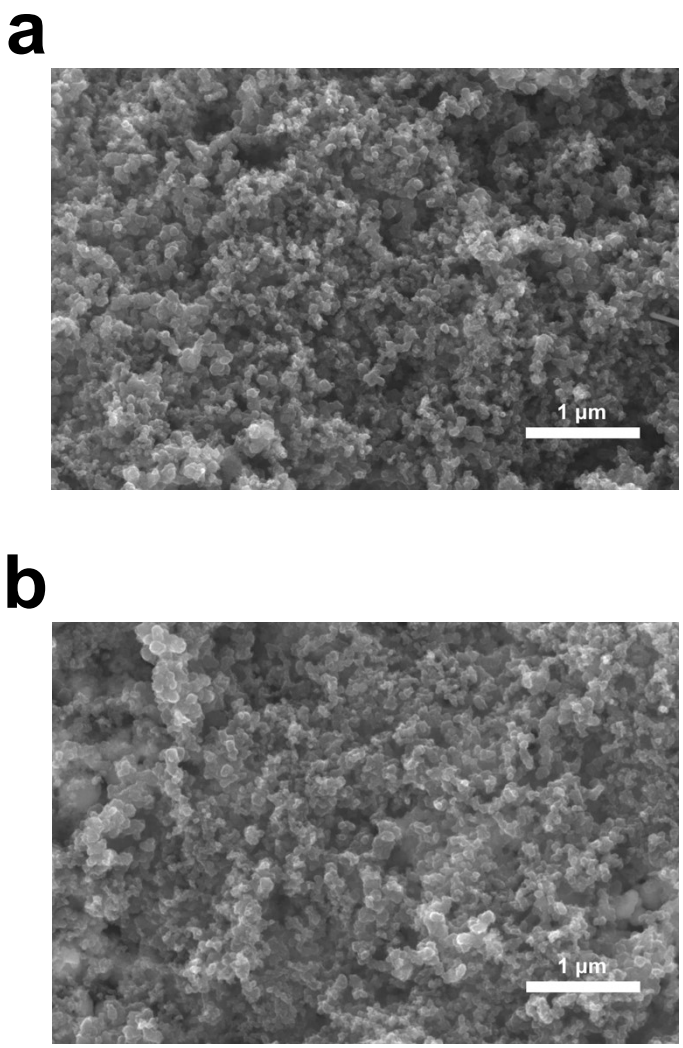

Fig. S19 Surface SEM images of the CB layer (a) before and (b) after CORR.

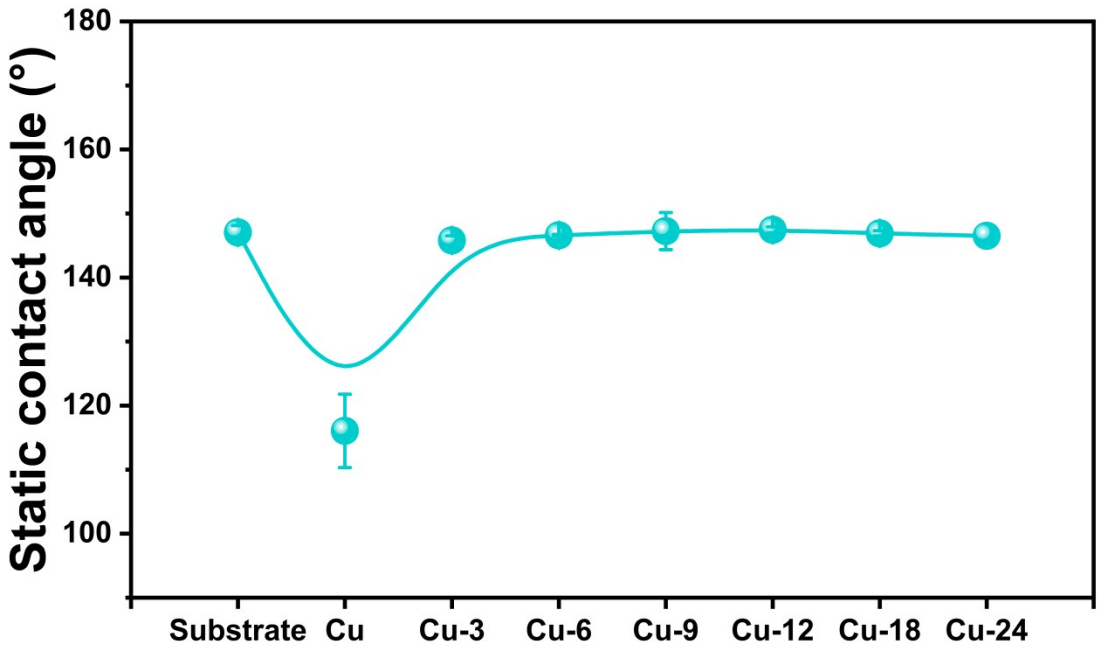

Fig. S20 Static contact angles on Cu-X surfaces. Substrate stands for bare carbon paper. Error bars represent the standard deviations of at least three independent measurements.

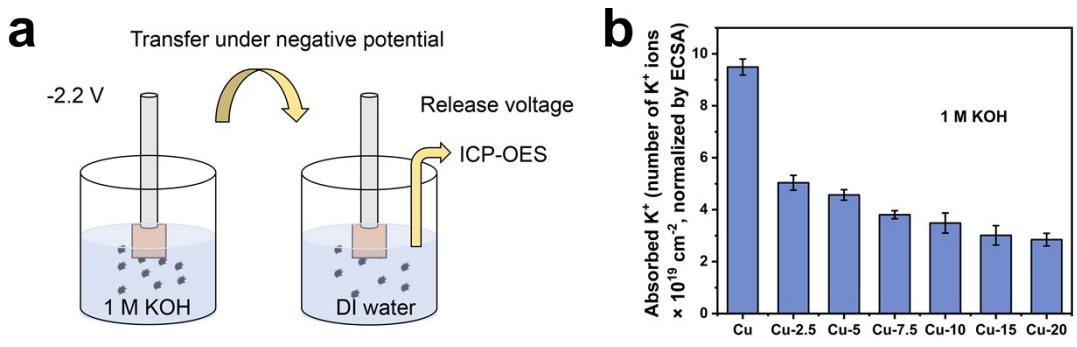

Fig. S21 Effect of carbon black layer on interfacial K^+ concentration. (a) Schematic of the K^+ retention measurement. (b) The adsorbed K^+ amount, normalized by the electrochemical surface area (ECSA).

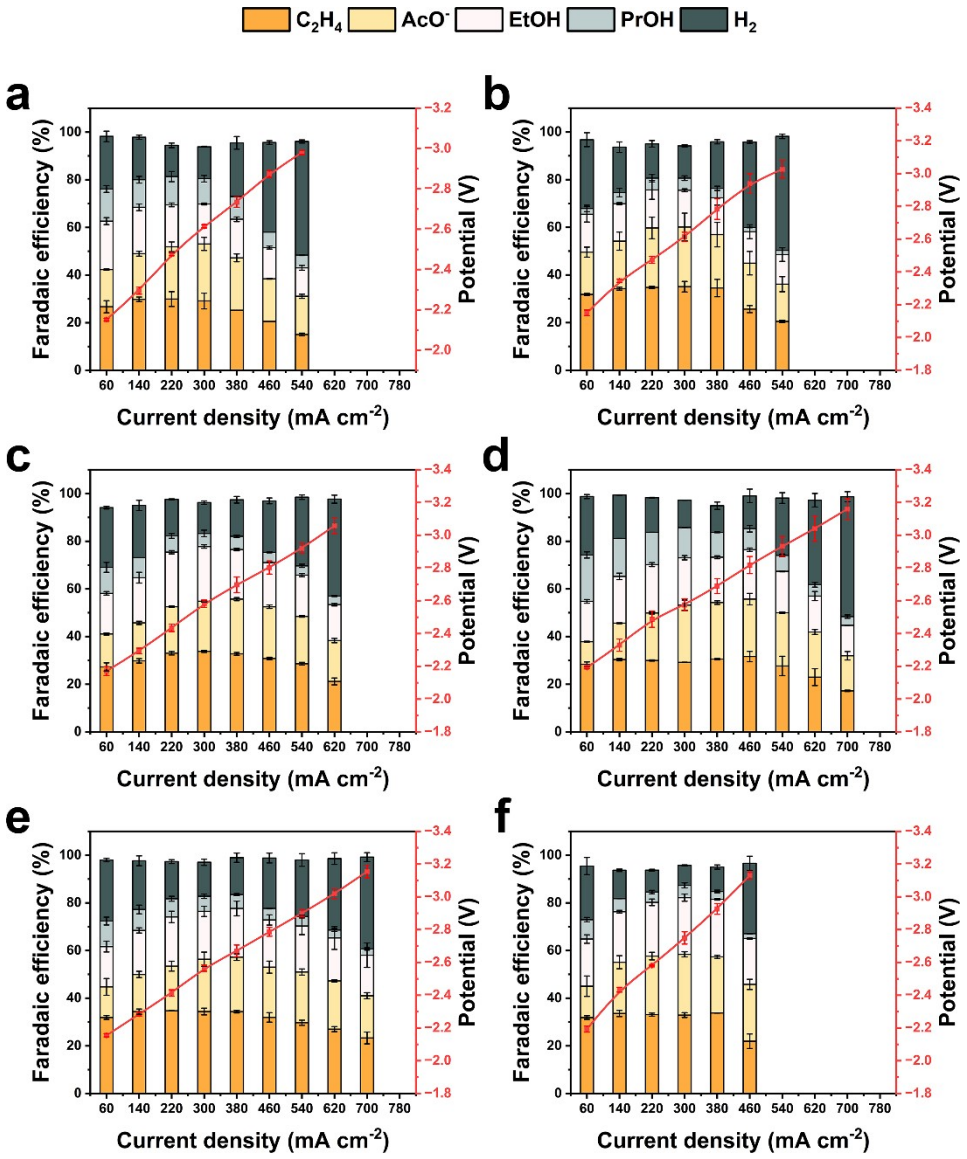

Fig. S22 The FEs of CORR products and H_2 on (a) Cu, (b) Cu-3, (c) Cu-6, (d) Cu-9, (e) Cu-18, and (f) Cu-24. The anolyte is 1 M KOH. Error bars represent the standard deviations of at least three independent measurements.

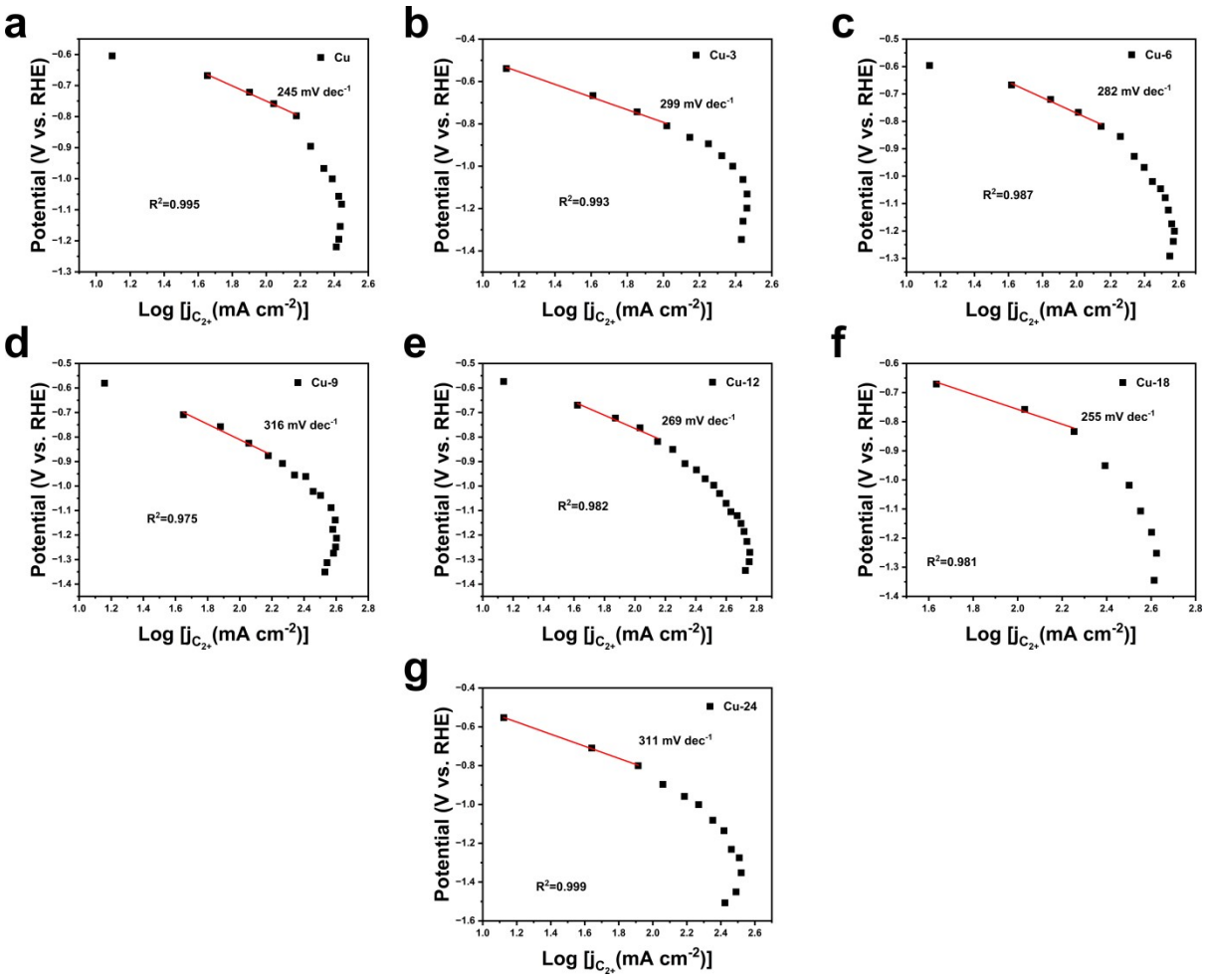

Fig. S23 The Tafel slopes of C_{2+} products on (a) Cu, (b) Cu-3, (c) Cu-6, (d) Cu-9, (e) Cu-12, (f) Cu-18, and (g) Cu-24. The anolyte is 1 M KOH.

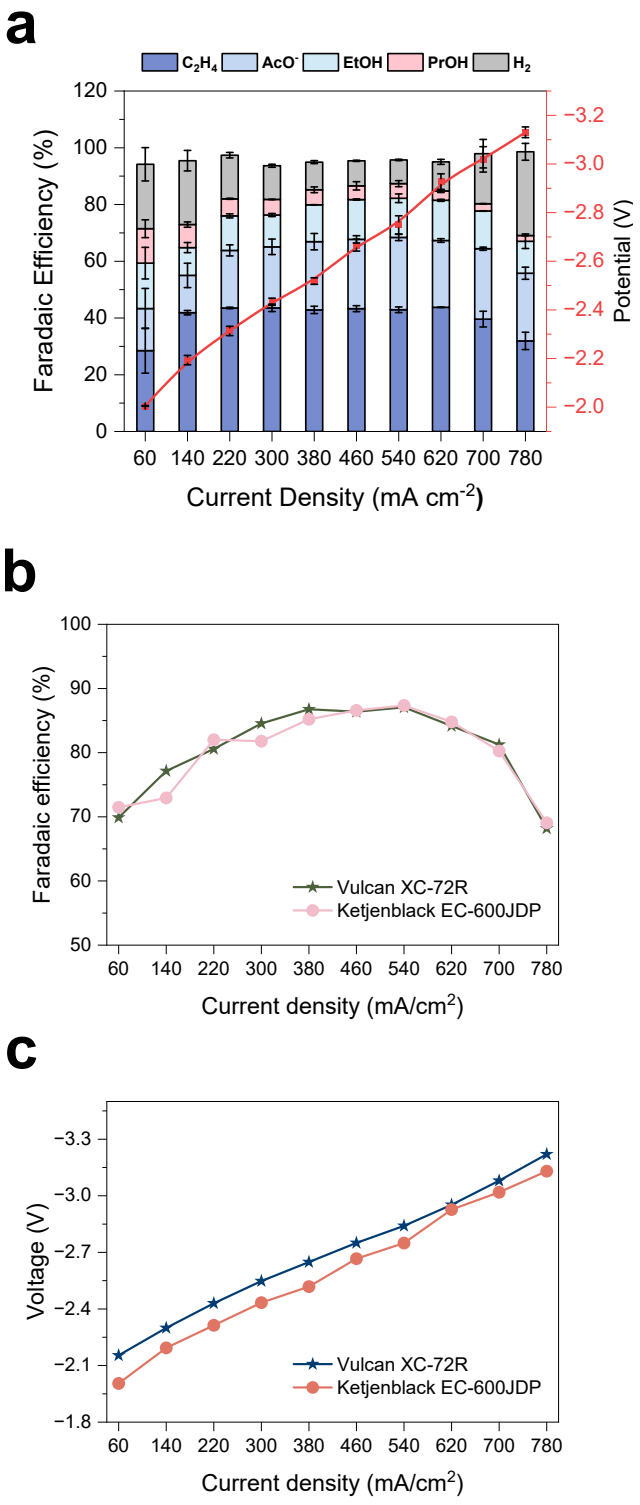

Fig. S24 (a) Product FEs and operating voltage for the Ketjenblack-based electrode, (b) Comparison of C_{2+} FE, (c) Comparison of cell voltage.

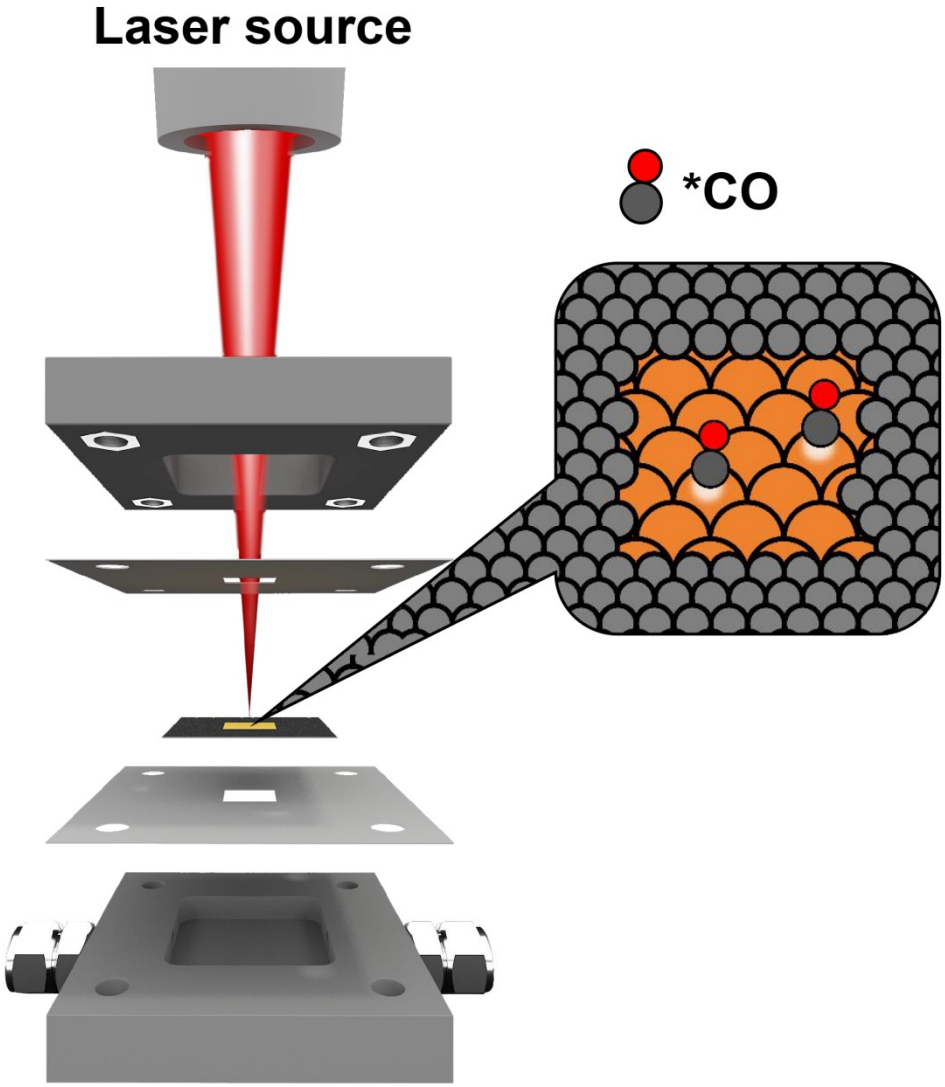

Fig. S25 A schematic diagram of the open flow cell for in-situ Raman studies.

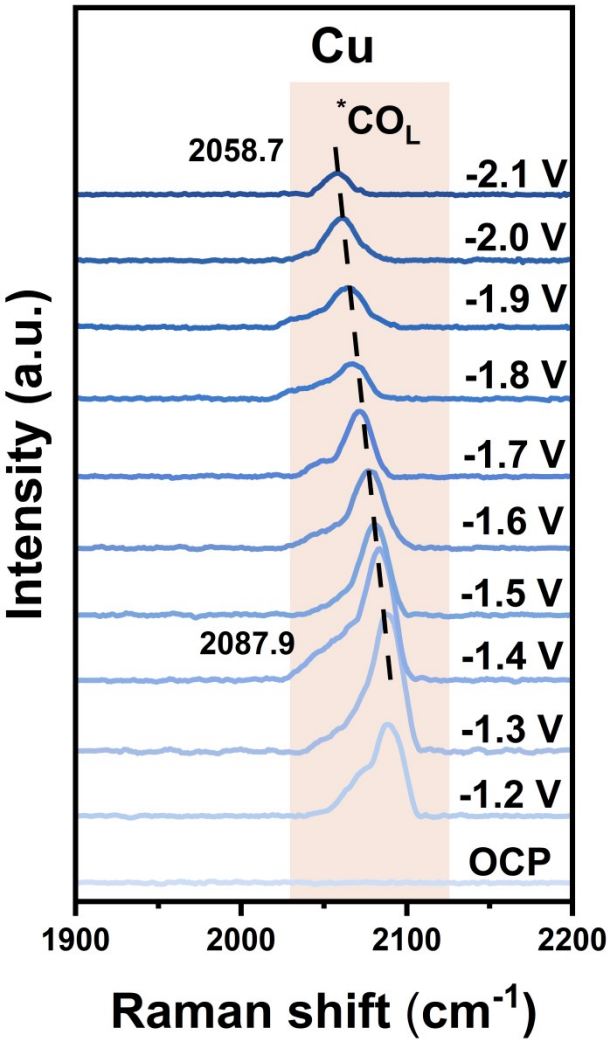

Fig. S26 In-situ Raman spectra collected on the Cu electrode using 1 M KOH anolytes.

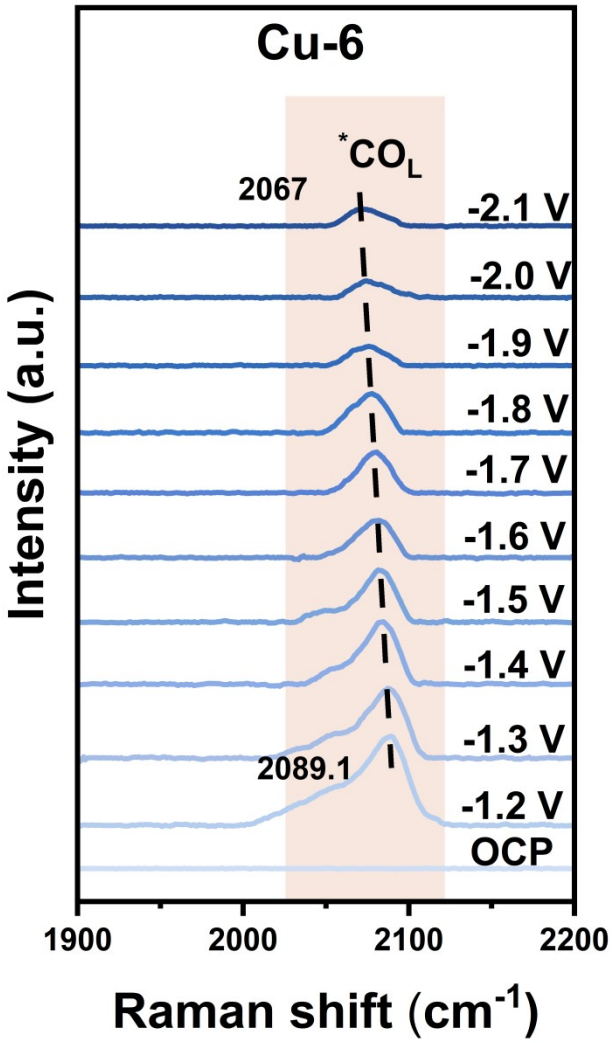

Fig. S27 In-situ Raman spectra collected on the Cu-6 electrode using 1 M KOH anolytes.

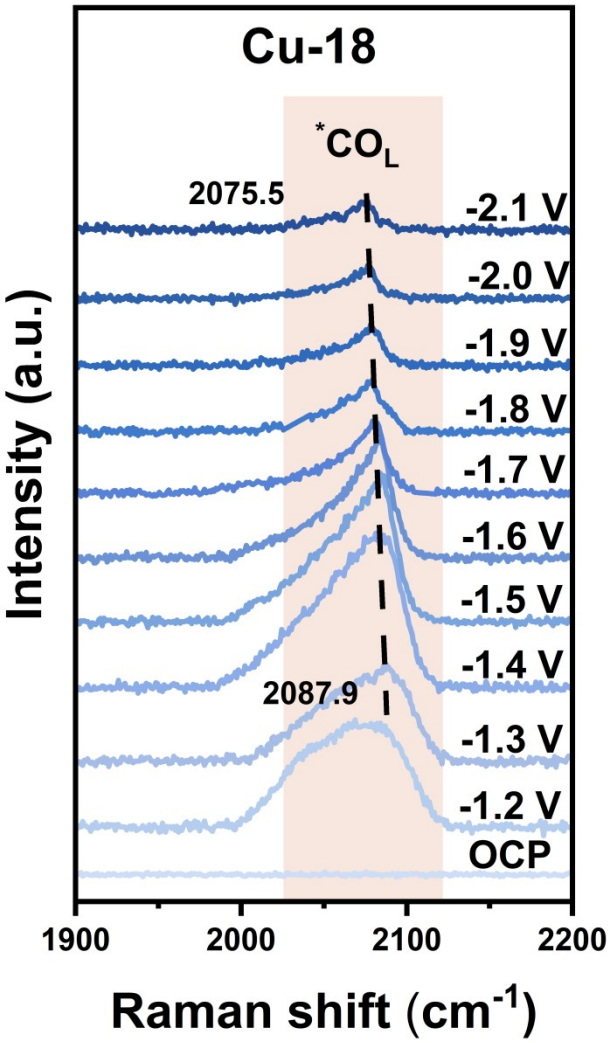

Fig. S28 In-situ Raman spectra collected on the Cu-18 electrode using 1 M KOH anolytes.

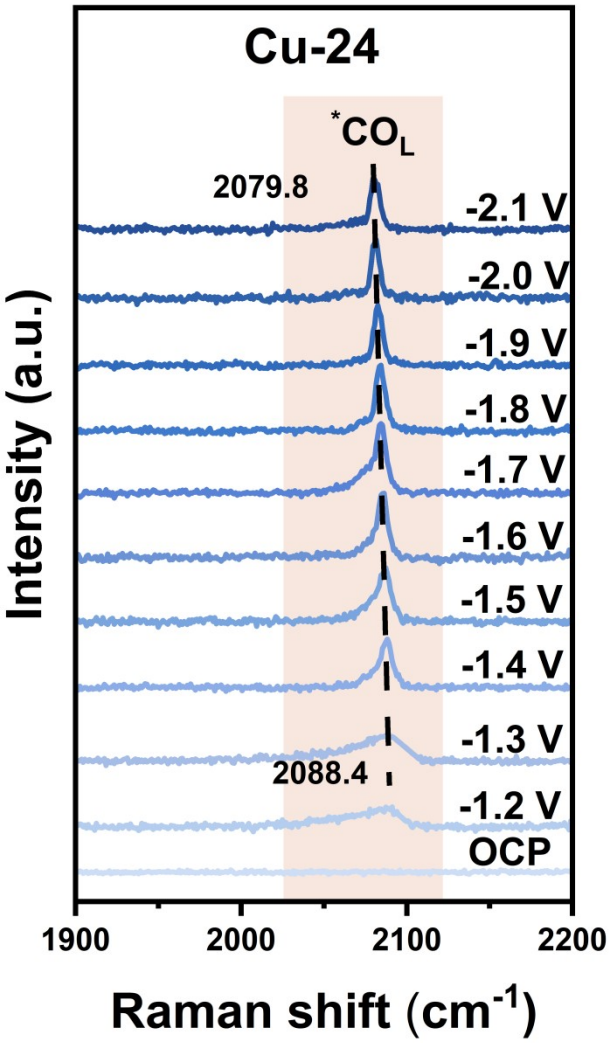

Fig. S29 In-situ Raman spectra collected on the Cu-24 electrode using 1 M KOH anolytes.

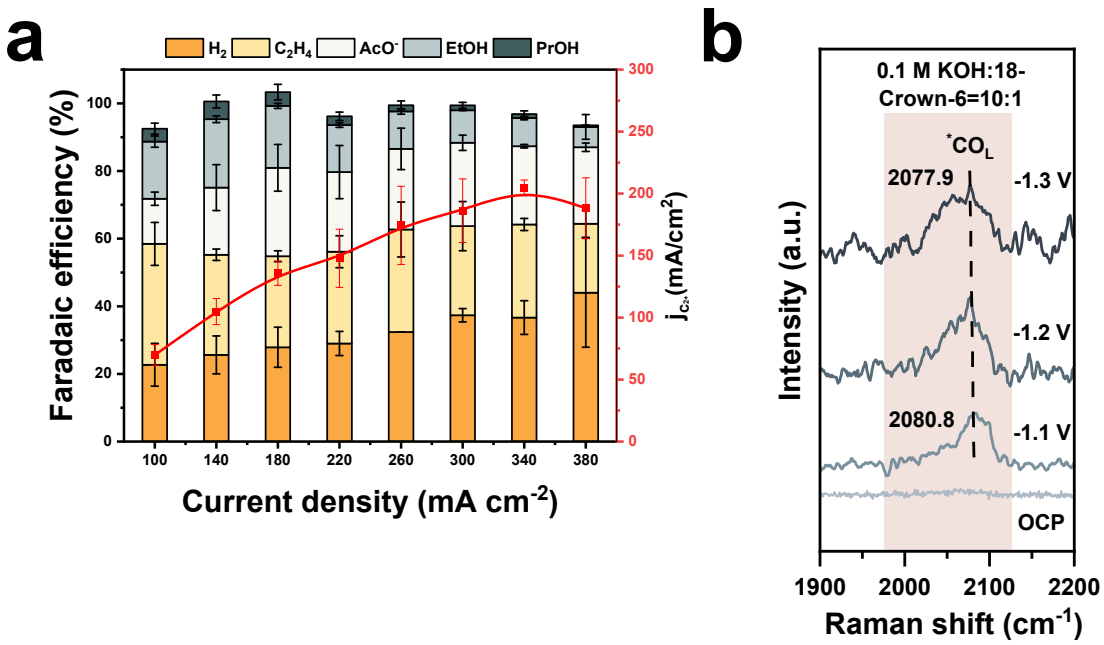

Fig. S30 Supporting data for the expanded volcano plot (Fig. 3c). (a) Faradaic efficiency (left axis) and C_{2+} partial current densities (right axis) measured at 100–380 mA cm^{-2} for 0.1 M KOH mixed with 18-Crown-6 at a 10:1 molar ratio. (b) In situ Raman spectra (1900–2200 cm^{-1} region) of adsorbed *CO_L and the corresponding linear fits for Stark tuning rate.

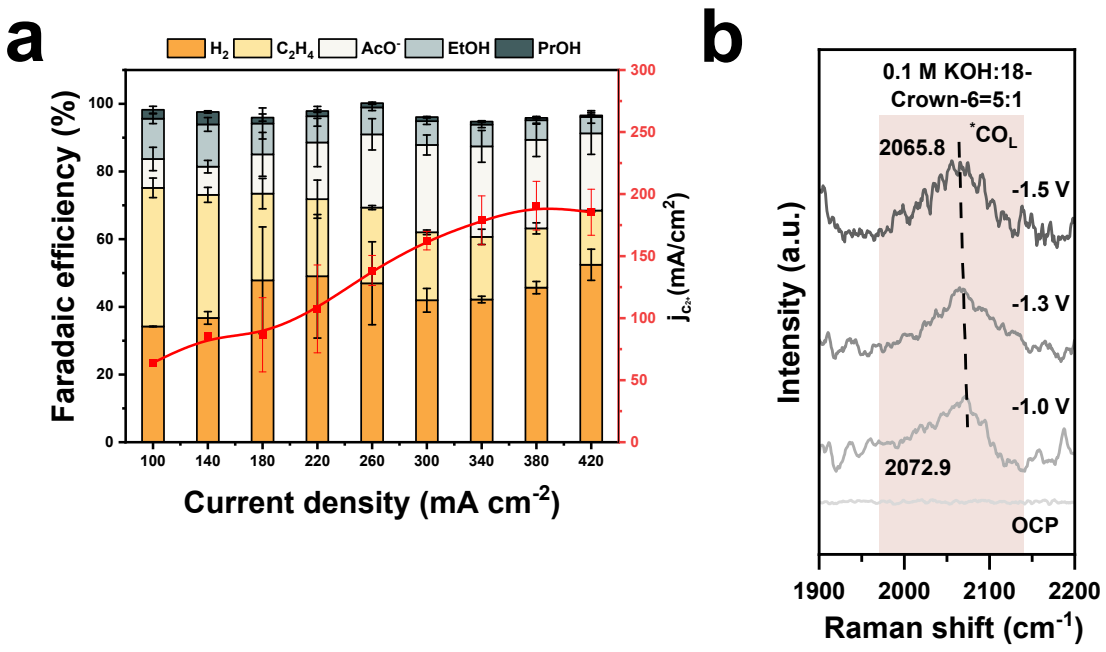

Fig. S31 Supporting data for the expanded volcano plot (Fig. 3c). (a) Faradaic efficiency (left axis) and C_{2+} partial current densities (right axis) measured at 100–420 mA cm^{-2} for 0.1 M KOH mixed with 18-Crown-6 at a 5:1 molar ratio. (b) In situ Raman spectra (1900–2200 cm^{-1} region) of adsorbed *CO_L and the corresponding linear fits for Stark tuning rate.

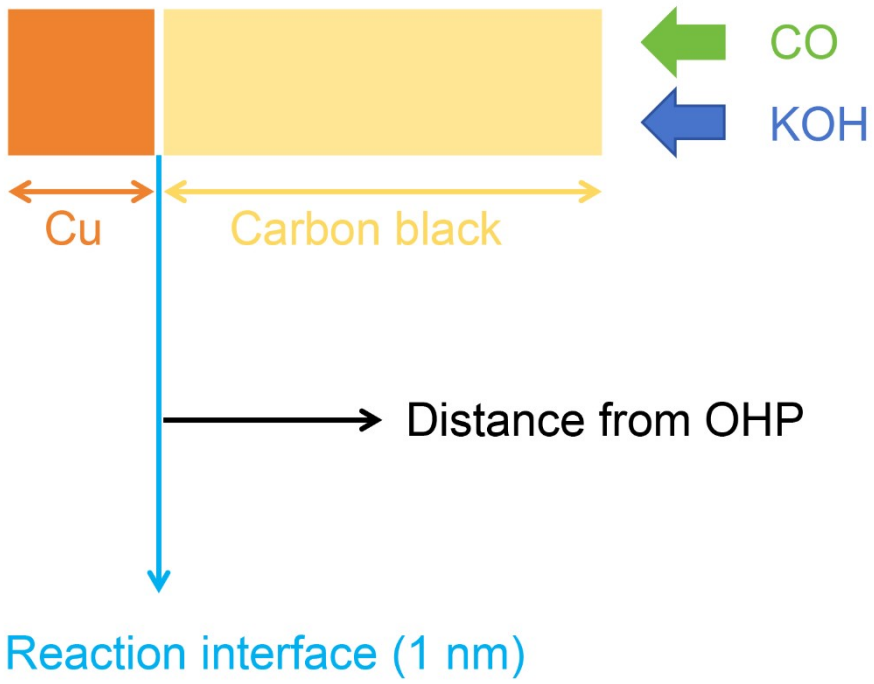

Fig. S32 The schematic illustration of the one-dimensional (1D) model. A reaction interface of 1 nm is defined to enable diffusion of K^+ and CO due to electromigration and CO reduction. CB layer with various thicknesses (i.e., 3, 6, 9, 12, 18, and 24 μm) is included to control the local concentrations of K^+ and CO.

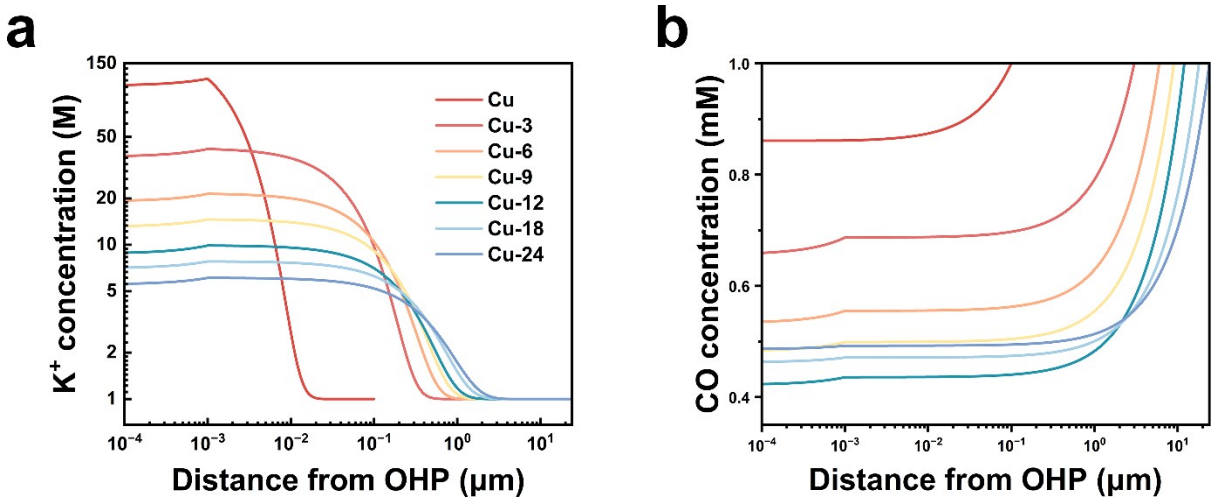

Fig. S33 The modeling results at 300 mA cm^{-2}. (a) The simulated concentration of K^+ on the Cu catalyst with different thicknesses of carbon black layers as a function of distance from the OHP at 300 mA cm^{-2}. (b) The simulated concentration of CO on the Cu catalyst with different thicknesses of CB layers as a function of distance from the OHP at 300 mA cm^{-2}.

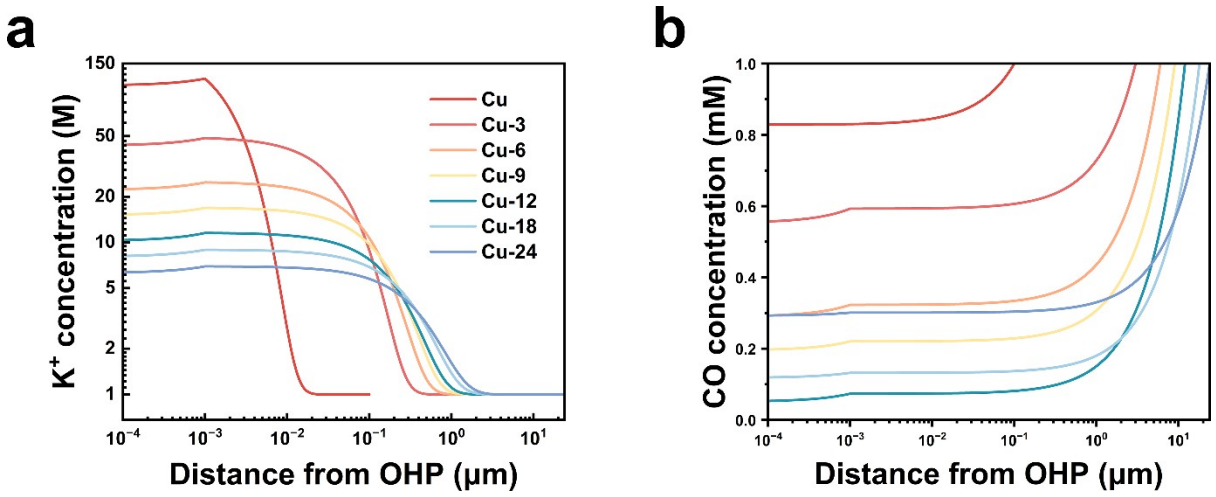

Fig. S34 The modeling results at 500 mA cm^{-2}. (a) The simulated concentration of K^+ on the Cu catalyst with different thicknesses of CB layers as a function of distance from the OHP at 500 mA cm^{-2}. (b) The simulated concentration of CO on the Cu catalyst with different thicknesses of CB layers as a function of distance from the OHP at 500 mA cm^{-2}.

Note S1. COMSOL simulations.

This section details the one-dimensional (1D) reaction-diffusion model developed to simulate the localized concentrations of K^+ ions and CO molecules within CB layers of varying thicknesses.

Geometric configuration

The model geometry comprises three key components: a Cu catalyst, a CB layer with variable thicknesses, and a 1 nm reaction-interfacial layer at their interface. At the right boundary of the porous carbon layer, a constant concentration of 1 M KOH electrolyte is imposed, while the dissolved CO concentration is initialized at 1 mM and maintained as a Dirichlet boundary condition. Electrical potentials are applied at the left boundary (Cu catalyst), and the right boundary is grounded to establish the electrical potential configuration. The thicknesses of the CB layers, estimated from experimental protocols, are systematically varied (3, 6, 9, 12, 18, and 24 μm) to investigate thickness-dependent mass transport phenomena. For simulations involving bare Cu electrodes, a 0.1 μm electrolyte domain is defined. The CB layer exhibits selective blocking capability toward K^+ ions, enabling explicit analysis of cation migration dynamics. A 1 nm OHP layer adjacent to the catalyst surface induces a high-density negative charge field, locally elevating K^+ concentrations to near-equilibrated levels within interfacial regions.

Physics configuration

Ohm's law governs current distribution within the cathodic catalyst layer. The catalyst domain is assumed to comprise a 0.4 copper catalyst volume fraction (8×10^4 S m^{-1}) and a 0.6 electrolyte volume fraction (4.56 Sm^{-1})[1].

$$i = -\sigma\frac{\partial \emptyset}{\partial x} \quad (1)$$

where σ is the electrical conductivity of different media, and the coordinate x defines the spatial position along the current flow direction.

The Nernst-Planck equation governs ion transport in electrolytes, comprising two governing components: an ion flux constitutive relation and a continuity equation derived from mass

conservation. The flux equation describes ionic diffusive-electromigration processes. The flux J_i of ion i is expressed as follows, including both diffusion and electromigration terms:

$$J_i = -D_i \nabla c_i - z_i u_{m,i} F c_i \nabla \emptyset \quad (2)$$

where D_i is the diffusion coefficient of ion i, ∇c_i is the concentration gradient of ion i, and z_i is the charge number of ion i. The $u_{m,i}$ is the mobility of ion i, $\nabla \emptyset$ is the gradient of the electric potential, indicating the strength and direction of the electric field.

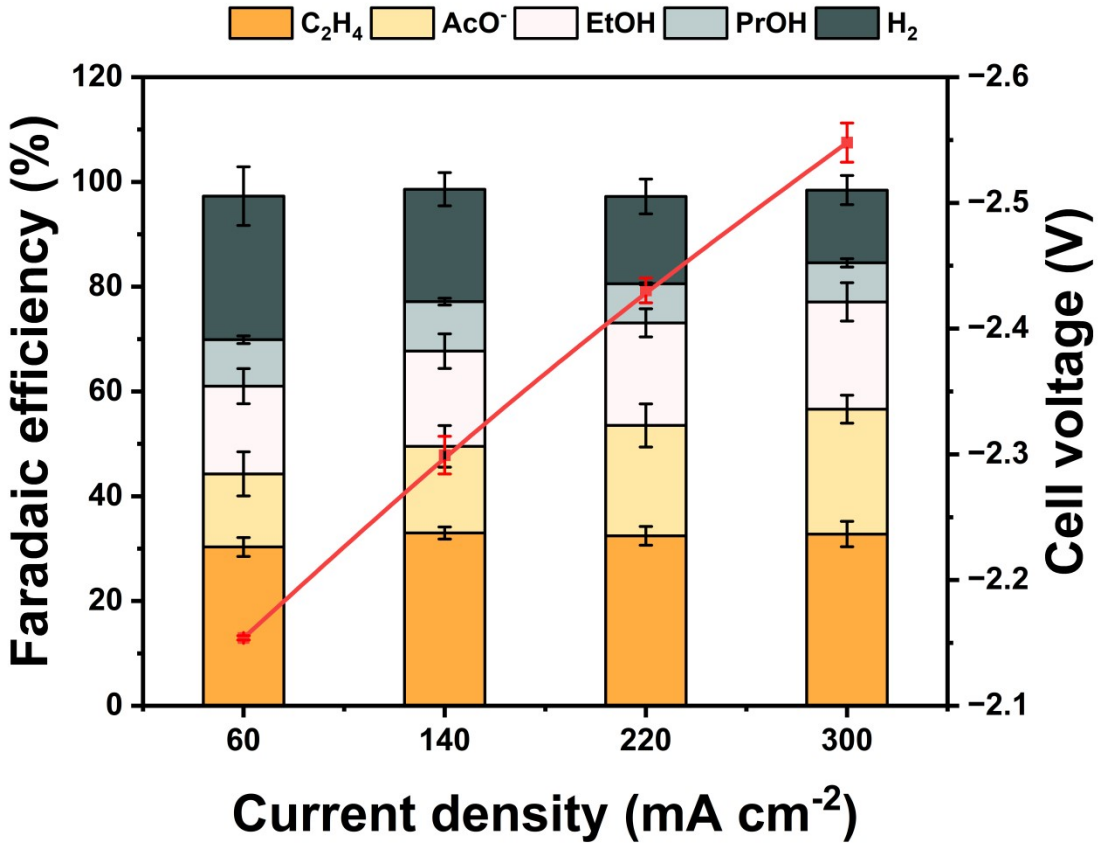

Fig. S35 FEs of CORR products and H_2 for the Cu-12 electrode from 60 to 300 mA cm^{-2} in a 5-cm^2 electrolyzer using 1 M KOH. Error bars represent the standard deviations of at least three independent measurements.

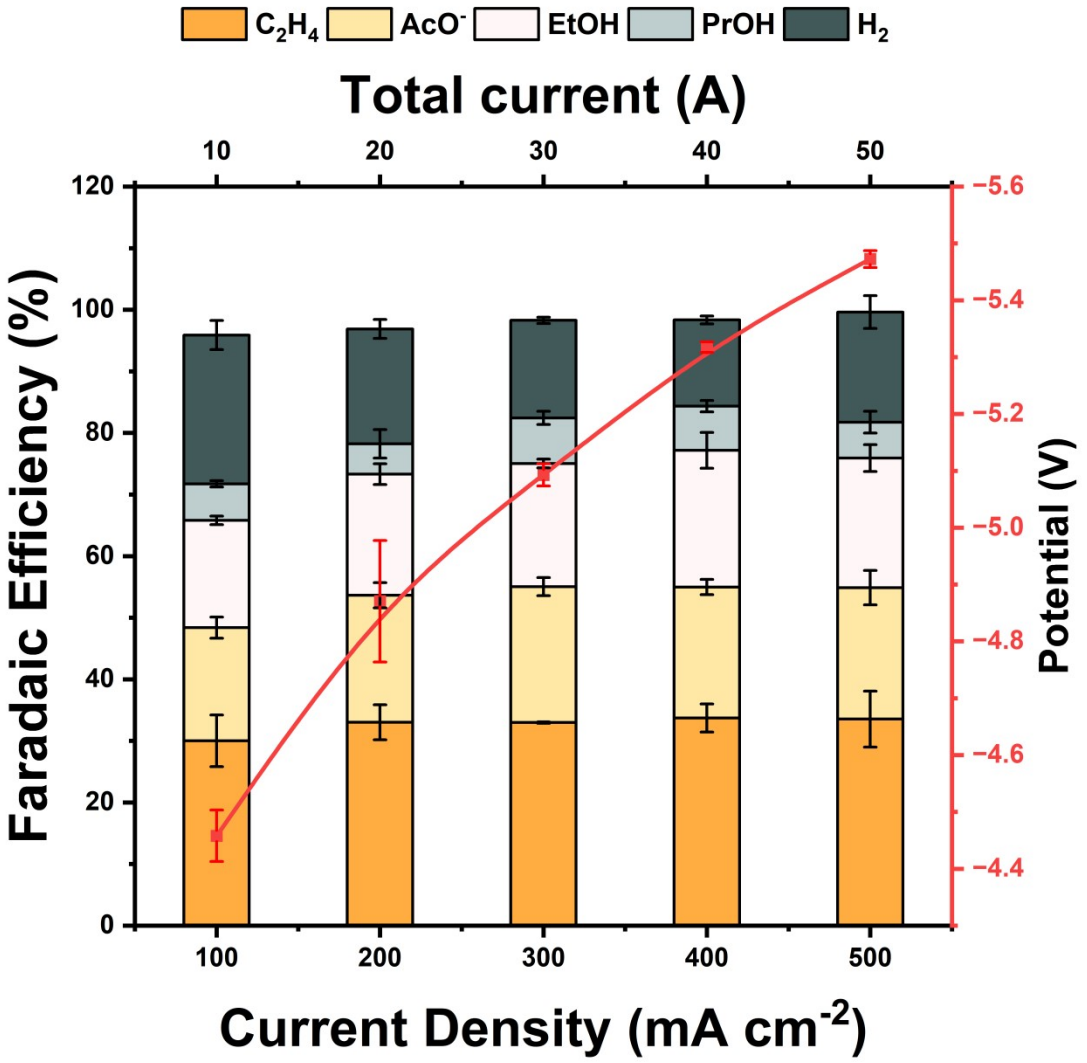

Fig. S36 CORR performance of an electrolyzer stack with a total reaction area of 2×50 cm^2. Error bars represent the standard deviations of at least three independent measurements.

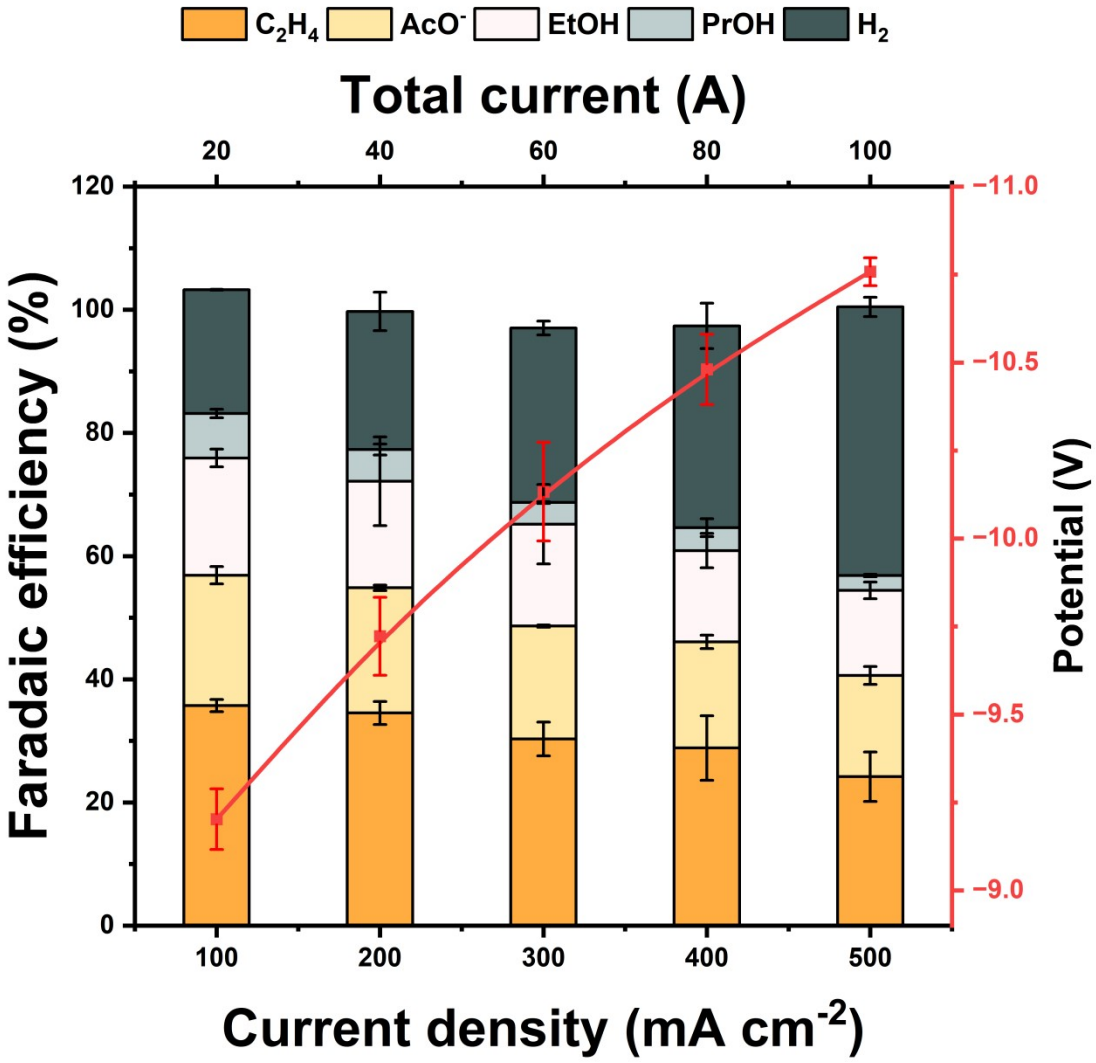

Fig. S37 CORR performance of an electrolyzer stack with a total reaction area of 4×50 cm^2. Error bars represent the standard deviations of at least three independent measurements.

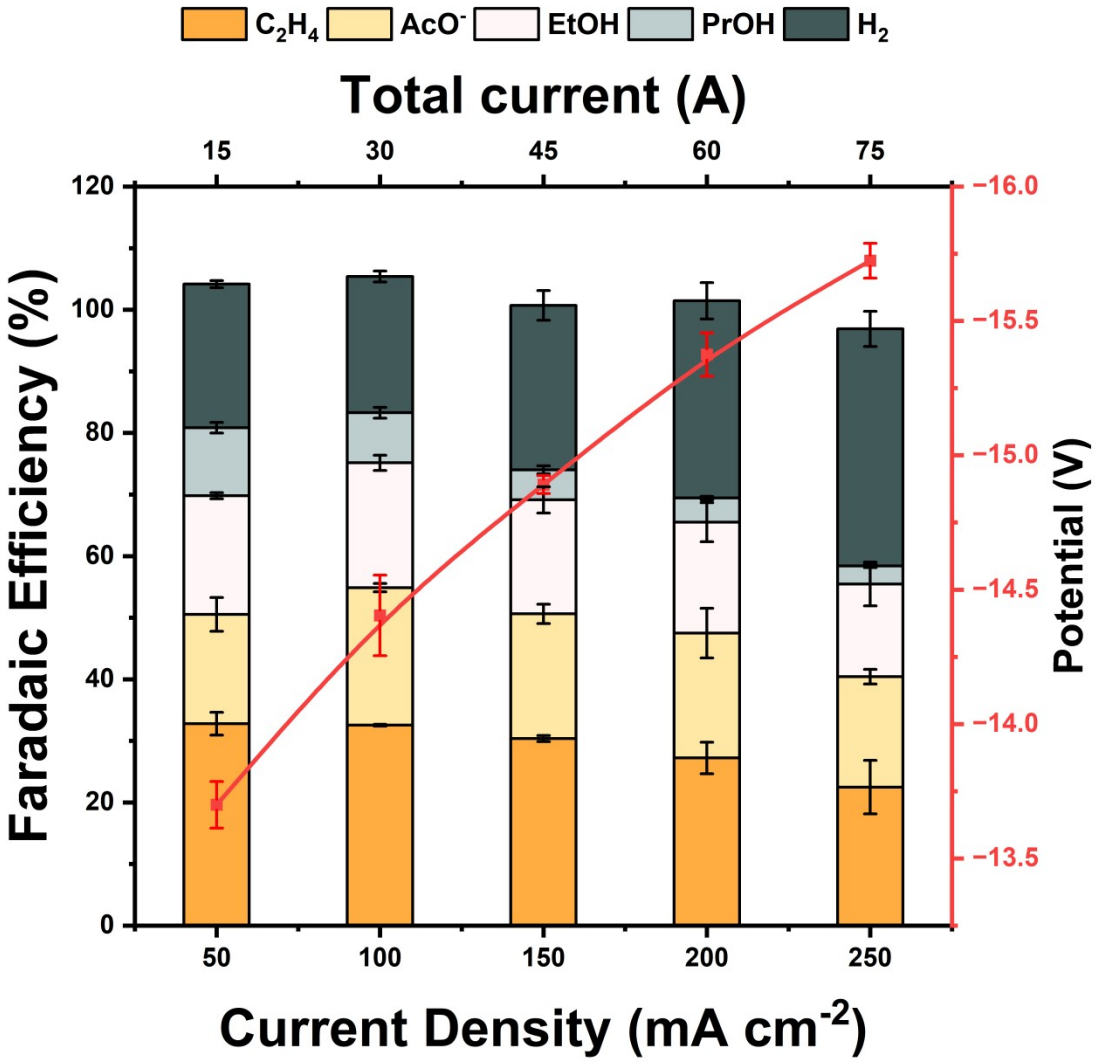

Fig. S38 CORR performance of an electrolyzer stack with a total reaction area of 6×50 cm^2. Error bars represent the standard deviations of at least three independent measurements.

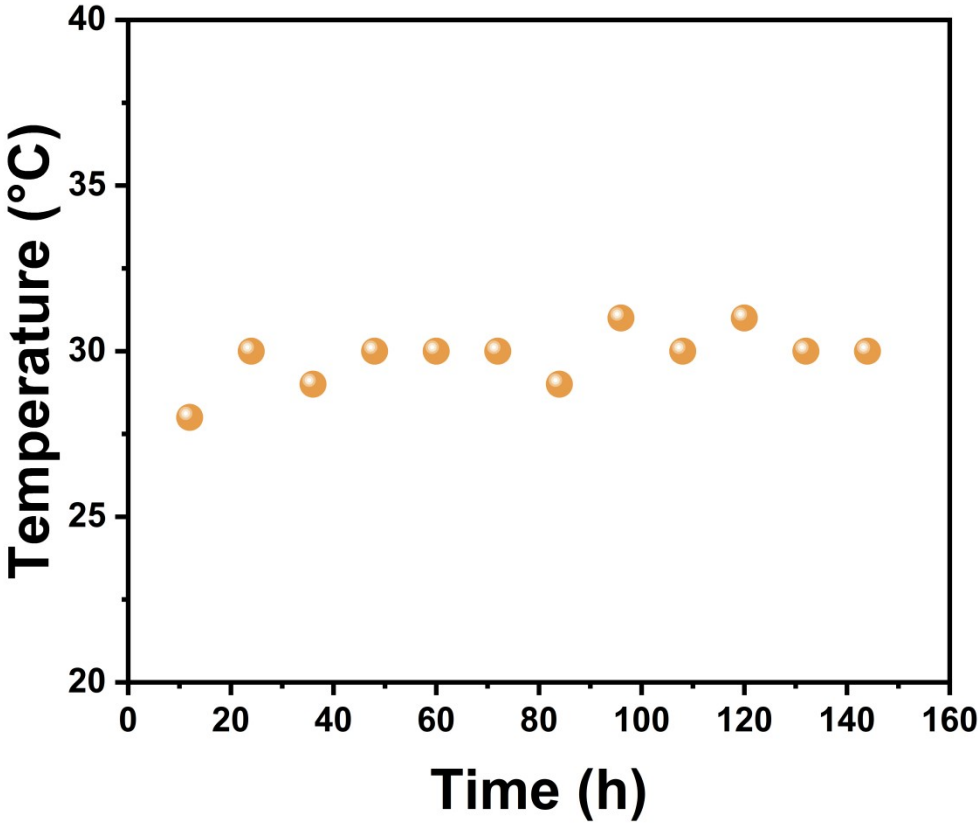

Fig. S39 The electrolyte temperature as a function of time during the 150-h operation at 92 W.

Table S1 Comparison of the present CORR performance advances to the best prior in MEA.

Catalyst	FE_{C2+} (%)	j_{C2+} (mA cm^{-2})	Stability and the corresponding current density (h@mA cm^{-2})	EE_{C2+} and the corresponding current density (%@mA cm^{-2})	Reference
Cu-12	87±2	569±5	180 h@400 mA cm^{-2}	33±0.4%@460 mA cm^{-2}	This work
Ag-Ru-Cu	93±3	540±18	102 h@300 mA cm^{-2}	33±1%@300 mA cm^{-2}	*Nat. Energy* 2022, **7**, 170–176
CCBH	87±2	598±20	200 h@200 mA cm^{-2}	19.6±1.2%@400 mA cm^{-2}	*Nat. Energy* 2023, **8**, 179–190
Cd-Cu (8 bar)	90±2	225±5	20 h@150 mA cm^{-2}	25%@250 mA cm^{-2}	*Nat. Commun.* 2024, **15**, 616
CuO-S20	93±2	465±10	100 h@500 mA cm^{-2}	22±1%@500 mA cm^{-2}	Angew. Chem. Int. Ed. 2024, **63**, e202412266
Pd-Cu	88±5	270±6	100 h@300 mA cm^{-2}	35±3%@200 mA cm^{-2}	*Nat. Commun.* 2023, **14**, 4882

Table S2 Physical properties of the carbon black materials used[2].

Parameter	Vulcan XC-72R	Ketjenblack EC-600JDP
BET specific surface area (m^2/g)	~254	~1400
Particle size (nm)	20-50	20-50
Iodine value (mL/100g)	~253	1000-1100
Bulk density (kg/m^3)	96	90-110

Table S3 Ionic diffusion coefficients of the electrolyte in the continuum transport models.

Species	Diffusion Coefficient (10^{-9} m^2 s^{-1})
CO	2.0
K^+	1.957
OH^-	5.273

References

[1] J. Yu, Y. Zheng, B. Lv, A. Huang, J. Zhang, Z. Wang, Y. Zhang, Y. Wu, Y. Zhou. Y. Wang and W. Luo, *Applied Catalysis B: Environment and Energy,* 2025, **368**, 125131.

[2] SCI Materials Hub, http://www.scimaterials.cn/ProDetail.aspx?ProId=633, (accessed Mau 2026).